

Near-threshold incoherent ϕ photoproduction on the deuteron: Searching for traces of a resonance

Alvin Kiswandhi,^{1,2} Shin Nan Yang,¹ and Yu Bing Dong^{3,4}¹*Department of Physics and Center for Theoretical Sciences, National Taiwan University, Taipei 10617, Taiwan*²*Department of Physics, STKIP Surya, Tangerang 15810, Indonesia*³*Institute of High Energy Physics, Chinese Academy of Sciences, Beijing 100049, China*⁴*Theoretical Physics Center for Science Facilities (TPCSF), CAS, Beijing 100049, China*

(Received 6 April 2016; published 28 July 2016)

We study the near-threshold incoherent ϕ photoproduction on the deuteron based on a model of $\gamma N \rightarrow \phi N$, consisting of Pomeron, (π, η) exchanges, and a $J^P = 3/2^-$ resonance, which describes the low-energy $\gamma p \rightarrow \phi p$ LEPS data well, including the peak in the forward differential cross section. The calculation is done up to double rescatterings, with the spin dependence of the elementary $\gamma N \rightarrow \phi N$ amplitude retained throughout the calculation. The Fermi motion and final-state interactions (FSIs) are all properly treated as prescribed by realistic nucleon-nucleon interaction. The couplings of the resonance to γn and ϕn channels are estimated with the help of a constituent quark model. The main features of the LEPS and CLAS data are described reasonably well except for some quantitative discrepancies at very low energies and low-momentum-transfer regions. It is found that contributions of Fermi motion, pn FSI, and resonance are all indispensable in bridging the differences between the single-scattering results and the data. The off-shell rescattering is found to be important because it cancels out a large portion of the on-shell contribution. The discrepancies at low-momentum-transfer regions might be related to the binning size of the data. No peak is found to be associated with the weak resonance because it gets smeared out by the Fermi motion and FSI with the deuterium target. The problem at very-low-energy regions hints at the possible contributions from other mechanisms and should be investigated in depth with the use of recent high-statistics $\gamma p \rightarrow \phi p$ data from CLAS.

DOI: [10.1103/PhysRevC.94.015202](https://doi.org/10.1103/PhysRevC.94.015202)

I. INTRODUCTION

It has long been established that the diffractive processes dominate the ϕ -meson photoproduction reaction at high energies and can be well described by t -channel Pomeron (P) exchange [1,2]. In the low-energy region, the nondiffractive processes of pseudoscalar (π, η) -meson exchanges are also known to contribute [1]. Other processes, such as nucleon exchange [3,4], nucleon resonances [5,6], second Pomeron exchange, t -channel scalar meson and glueball exchanges [6,7], and $s\bar{s}$ -cluster knockout [4,8,9], have also been suggested and studied. However, no definite conclusion has been inferred because of the limited experimental data. Recently, a nonmonotonic behavior in the differential cross sections (DCSs) of ϕ photoproduction on proton at forward angles around $E_\gamma \sim 2.0$ GeV has been observed by the LEPS Collaboration [10] and confirmed by the new high-statistics data from CLAS [11,12]. It cannot be explained by the processes mentioned above.

We found in Refs. [13,14] that, with an addition of a resonance of spin parity $J^P = 3/2^-$, with mass $M = 2.10 \pm 0.03$ GeV and width $\Gamma = 0.465 \pm 0.141$ GeV to the background mechanisms, which consist of Pomeron and (π, η) -meson exchanges in the t channel, not only the peak in the forward differential cross section but also the t dependence of DCS, ϕ -meson decay angular distribution, and the spin-density matrix elements (SDMEs) can be well described. It would hence be of interest to see how such a postulated resonance would exhibit itself in other reactions, like ϕ -meson photoproduction from deuterium at low energies.

Data on incoherent photoproduction of ϕ mesons from deuteron at low energies have recently become available from the LEPS [15,16] and CLAS [17] Collaborations. While CLAS [17] measured only the DCSs and the decay angular distributions of ϕ meson, LEPS provided more extensive data. With a linearly polarized photon beam, they were able to measure the decay asymmetries and SDMEs, in addition to the DCSs [15,16]. This prompts us to set forth to confront our model of Refs. [13,14] with these recent extensive data to see whether it is possible to mine this postulated resonance from them. This is clearly a daunting task because the strength of this postulated resonance was found to be relatively weak and can be marred by Fermi motion, final-state interactions (FSIs) of the nucleons, meson rescattering effects, and production via neutron.

The LEPS [15,16] and CLAS [17] data are recently analyzed in Ref. [18], where the Fermi motion is taken into account for the single-scattering calculation and the effects of the rescatterings of ϕN and NN in the final state are also investigated. It is found there that both the Fermi motion and the FSI of the nucleons give non-negligible contributions, while the double scattering of the ϕ meson with nucleons can be neglected. Because we are interested in finding possible traces of the postulated resonance, which is rather weak, from other reactions like ϕ -meson photoproduction from deuteron, a very careful treatment of the reaction is hence essential.

Consequently, in addition to the inclusion of the postulated resonance, we implement the following improvements over the calculation of Ref. [18]. First is that the spin structure

of the elementary $\gamma N \rightarrow \phi N$ amplitude, including those of the Pomeron and t -channel (π, η) exchanges, is retained. The spin-dependent part of the Pomeron-exchange amplitude was extensively studied in Ref. [6] and found to be responsible for the spin-flip transitions at forward production angles and appears in the angular distributions of ϕ decay with both unpolarized and polarized photon beams. In the present case of incoherent ϕ production from deuteron, SDMEs would be either a constant or zero. The inclusion of the spin-dependent part of the elementary amplitude will provide a useful probe for the resonance and deeper insight into the reaction mechanism. Second, the t -channel (π, η) exchanges are included. This is important because we found in Ref. [18] that the nonmonotonic structure observed in the cross section of $\gamma p \rightarrow \phi p$ is enhanced by the interference of resonance and π -exchange contributions. Last, the rescattering effects between nucleons are estimated with the realistic Nijmegen NN interactions [19,20], which ensure that the two-body unitarity is satisfied. Besides, the D state in the deuteron and the off-shell rescattering are also taken into account. All of these were overlooked in Ref. [18].

Reactions with a deuteron target are often used to extract the corresponding elementary reaction amplitude from a neutron. However, in this study, we use isospin invariance to infer the ϕ production amplitude from neutron as much as possible. Because it is known that a Pomeron behaves like an isoscalar particle, the Pomeron-exchange amplitude is taken to be the same as that with a proton. For the t -channel (π, η) exchanges, isospin symmetry allows us to write the corresponding amplitude with a neutron. The only unknown quantity in our model is the excitation strength of the resonance from a neutron. For our present purpose, we take it to be similar to a resonance with the same spin-parity and roughly the same mass, as well as assume that it has the same ratio of the proton helicity amplitudes predicted by a constituent quark model of Ref. [21]. The details are expounded in Appendix A. With this choice, our results are free from any fitting to the $\gamma d \rightarrow \phi pn$ DCS and SDME data obtained by the LEPS and CLAS Collaborations [15–17] and some of these results were reported in Ref. [22].

This paper is organized as follows. In Sec. II we present the details of our calculations. The elementary $\gamma N \rightarrow \phi N$ amplitude is first briefly described. Then the ϕ production amplitudes via single and double-scattering mechanisms with deuteron targets are given. In Sec. III results are shown and discussed. A summary and conclusions are presented in Sec. IV. Some details of our calculations are given in the appendixes for clarity.

II. THE MODEL FOR $\gamma d \rightarrow \phi pn$ REACTION

In this section, we present the essentials of our calculations. The kinematics and the notations are first introduced. Then the elementary amplitude for photoproduction of a ϕ meson from nucleon, $\gamma N \rightarrow \phi N$, the basis of our calculation, is briefly discussed with details given in Appendix A. Last, we explain the details of our calculations regarding how the Fermi motion and final-state rescattering with both on- and off-shell ones are treated.

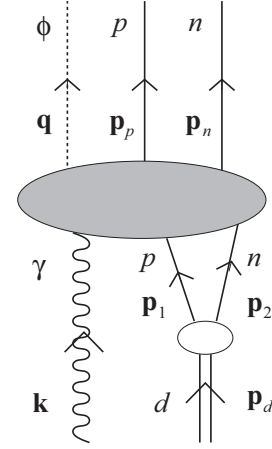


FIG. 1. The $\gamma d \rightarrow \phi pn$ reaction with $\gamma(\mathbf{k})$, $\phi(\mathbf{q})$, $d(\mathbf{p}_d)$, $p(\mathbf{p}_p)$, and $n(\mathbf{p}_n)$ denote the photon, ϕ meson, deuteron, proton, and neutron lines, respectively, with their momenta given inside the brackets. Also, \mathbf{p}_1 (\mathbf{p}_2) denotes the initial proton (neutron) momenta inside the deuteron. It should be emphasized that the ellipse joining the deuteron, proton, and neutron lines is not an interaction vertex.

A. Kinematics

Let us first introduce the momenta of the particles involved in the reaction. Here k , p_d , q , p_p , and p_n are the four-momenta of the photon, deuteron, ϕ meson, proton, and neutron, respectively, while p_1 (p_2) is that of the proton (neutron) inside the deuteron, as shown in Fig. 1. Notice also that $k = (E_\gamma, \mathbf{k})$, $q = (E_\phi, \mathbf{q})$, and $p_a = (E_a, \mathbf{p}_a)$, where $a = p, n, d$. The masses of the deuteron, ϕ meson, proton, and neutron are denoted by M_d , M_ϕ , M_p , and M_n , respectively. We work in the laboratory (LAB) frame where the deuteron is at rest. In this study, we use the plane-wave normalization that reads $\langle \mathbf{p}' | \mathbf{p} \rangle = (2\pi)^3 2E_p \delta^{(3)}(\mathbf{p}' - \mathbf{p})$ and $\bar{u}(\mathbf{p}, s) u(\mathbf{p}, s) = 2M$ for a Dirac spinor with mass M . In addition, we introduce

$$\langle f | \hat{T} | i \rangle = (2\pi)^4 \delta^{(4)}(k + p_d - q - p_p - p_n) \mathcal{M}_{fi}, \quad (1)$$

where the S matrix is given by $\hat{S} = \hat{I} - i\hat{T}$. The invariant amplitude $-i\mathcal{M}_{fi}$ is obtained diagrammatically with Feynman rules.

For later convenience, we define the Mandelstam variables s , t_ϕ , and u_ϕ as

$$\begin{aligned} s &= (k + p_d)^2 = (q + p_p + p_n)^2, \\ t_\phi &= (q - k)^2 = (p_d - p_p - p_n)^2, \\ u_\phi &= (q - p_d)^2 = (k - p_p - p_n)^2, \end{aligned} \quad (2)$$

and

$$s + t_\phi + u_\phi = M_d^2 + M_\phi^2 + M_{pn}^2, \quad (3)$$

where M_{pn} is the invariant mass of the pn system in the final state. For a fixed value of t_ϕ , M_{pn} has the minimum and maximum values of

$$\begin{aligned} M_{pn}^{\min} &= M_p + M_n, \\ M_{pn}^{\max} &= \sqrt{s + M_\phi^2 - 2\sqrt{s} E'_\phi}, \end{aligned} \quad (4)$$

with

$$E'_\phi \equiv \sqrt{M_\phi^2 + q'^2},$$

$$q' \equiv \frac{M_\phi^2 - t_\phi}{4E_\gamma^{\text{c.m.}}} - \frac{M_\phi^2 E_\gamma^{\text{c.m.}}}{M_\phi^2 - t_\phi}. \quad (5)$$

The value of u_ϕ is in turn limited to be within

$$u_{\phi,\text{min}} = M_d^2 + M_\phi^2 + (M_p + M_n)^2 - s - t_\phi,$$

$$u_{\phi,\text{max}} = M_d^2 + 2M_\phi^2 - 2\sqrt{s}E'_\phi - t_\phi, \quad (6)$$

and the value of t_ϕ is also restricted within

$$t_{\phi,\text{min}} = M_\phi^2 - 2E_\gamma^{\text{c.m.}}(E_{\phi,\text{max}} - q_{\text{max}}),$$

$$t_{\phi,\text{max}} = M_\phi^2 - 2E_\gamma^{\text{c.m.}}(E_{\phi,\text{max}} + q_{\text{max}}), \quad (7)$$

where $E_\gamma^{\text{c.m.}}$ is the photon energy in the γd center-of-mass (c.m.) frame and

$$q_{\text{max}} \equiv \sqrt{\frac{[s - (M_\phi + M_{pn}^{\text{min}})^2][s - (M_\phi - M_{pn}^{\text{min}})^2]}{4s}},$$

$$E_{\phi,\text{max}} \equiv \sqrt{M_\phi^2 + q_{\text{max}}^2}, \quad (8)$$

which corresponds to the case where the three-momentum of the ϕ meson in the c.m. system achieves its maximum value which clearly happens only when M_{pn} is in its minimum.

The differential cross section of $\gamma d \rightarrow \phi pn$ in the LAB system is

$$\frac{d\sigma_d}{dt_\phi} = \frac{1}{128E_\gamma^2 M_d^2} \frac{1}{(2\pi)^4} \int_{u_{\phi,\text{min}}}^{u_{\phi,\text{max}}} du_\phi \frac{P_p^{c,pn}}{M_{pn}}$$

$$\times \int d\Omega_p^{c,pn} \sum_{\lambda} \sum_{\lambda'} |\mathcal{M}_{fi}|^2, \quad (9)$$

where λ (λ') denotes the initial (final) spins, and $\mathbf{p}_p^{c,pn} = (p_p^{c,pn}, \Omega_p^{c,pn})$ denotes the three-momentum of the final proton in the c.m. system of the final pn system.

B. The elementary $\gamma N \rightarrow \phi N$ amplitudes

The basic input in our model is the elementary amplitude of ϕ -meson photoproduction from a free nucleon, $\mathcal{M}_{\gamma N \rightarrow \phi N}$ in which $N = p, n$. In our study, the amplitude $\mathcal{M}_{\gamma p \rightarrow \phi p}$ constructed in our previous work [14] will be employed. It consists of nonresonant and resonant amplitudes. The nonresonant amplitude consists of Pomeron and (π, η) exchanges in the t channel. The resonant amplitude arises from a postulated $J^P = 3/2^-$ resonance contribution. Notice that the contribution from the u -channel amplitude is very small and in this work we include only the s -channel contribution. The details of the model are given in Appendix A. The values for the mass, width, and coupling constants for the $J^P = 3/2^-$ resonance, as determined in Ref. [14], are presented in Table I.

For the production amplitude from neutron $\mathcal{M}_{\gamma n \rightarrow \phi n}$, the P and (π, η) t -channel exchange amplitudes can be readily written with the assumption of isospin symmetry. However, the resonance couplings to γn and ϕn channels have yet to be determined because there are no data on $\gamma n \rightarrow \phi n$ available.

TABLE I. The N^* mass, width, and coupling constants for $J^P = 3/2^-$ resonances.

	Proton ($N = p$)	Neutron ($N = n$)
M_{N^*} (GeV)		2.08
Γ_{N^*} (GeV)		0.570
$g_{\gamma NN^*}^{(1)}$	0.0323	-0.0441
$g_{\gamma NN^*}^{(2)}$	0.0420	-0.0193
$g_{\phi NN^*}^{(1)}$		-20.94
$g_{\phi NN^*}^{(2)}$		-2.61
$g_{\phi NN^*}^{(3)}$		-3.36

For our present purpose, we determine their values according to the following recipe. Namely, we first assume that the electromagnetic excitation of the resonance, hence its ratio of helicity amplitudes $A_{1/2}^p/A_{3/2}^p$ for γp , would be similar to that of a $J^P = 3/2^-$ nucleon state with roughly the same mass as predicted by a theoretical model. We take it as the $J^P = 3/2^-$ nucleon state with a bare mass of 2095 MeV and a positive value for the ratio of helicity amplitudes $A_{1/2}^p/A_{3/2}^p$ for γp decay, as predicted in the constituent quark model (CQM) of Ref. [21]. For the resonance coupling with the ϕn channel, we assume that they are identical to that with the ϕp channel because ϕ is an isoscalar particle. The details of the determination of the coupling constants $g_{\gamma nn^*}^{(i)}$ and $g_{\phi nn^*}^{(j)}$ of γnn^* and ϕnn^* vertices are presented in Appendix A.

Note that the Pomeron-exchange amplitude as given in Eq. (A2) depends on the polarizations of both the incident photon and outgoing ϕ meson, which were neglected in Ref. [18]. The π - and η -exchange amplitudes were also not included in Ref. [18].

C. $\gamma d \rightarrow \phi pn$ amplitudes

Within the multiple-scattering scheme, the diagrams for the $\gamma d \rightarrow \phi pn$ reaction up to triple rescatterings are shown in Fig. 2. Figure 2(a) is the single-scattering diagram, Fig. 2(b) is the double-scattering diagram with rescatterings between the final nucleons, and Fig. 2(c) is the double-scattering diagram with rescatterings between meson M produced by the incoming photon and final nucleon. Figures 2(d) and 2(e) represent the triple-scattering diagrams. In this work, we consider only up to the single-scattering and pn double-scattering diagrams of Figs. 2(a) and 2(b), because Fig. 2(c) with $M = \pi, \eta, \rho, \omega, \phi, \dots$ was studied in Ref. [18] and found to be small.

In general, the amplitude for $\gamma d \rightarrow \phi pn$ can be expressed as

$$\mathcal{M}_{fi} = \sum_{m_1, m_2} \int \frac{d^3 p_1}{(2\pi)^3} \frac{d^3 p_2}{(2\pi)^3} \frac{1}{2E_1} \frac{1}{2E_2}$$

$$\times \mathcal{M}_{\gamma pn}(\mathbf{k}, \mathbf{p}_1, \mathbf{p}_2, m_\gamma, m_1, m_2; \mathbf{q}, \mathbf{p}_p, \mathbf{p}_n, m_\phi, m_p, m_n)$$

$$\times \langle \mathbf{p}_1, \mathbf{p}_2; m_1, m_2 | \mathbf{p}_d, \Phi_d; m_d \rangle, \quad (10)$$

where the momenta of the particles are defined in Fig. 1 and the internal structure of the deuteron is characterized by its wave function Φ_d . The spin projections of the particles are

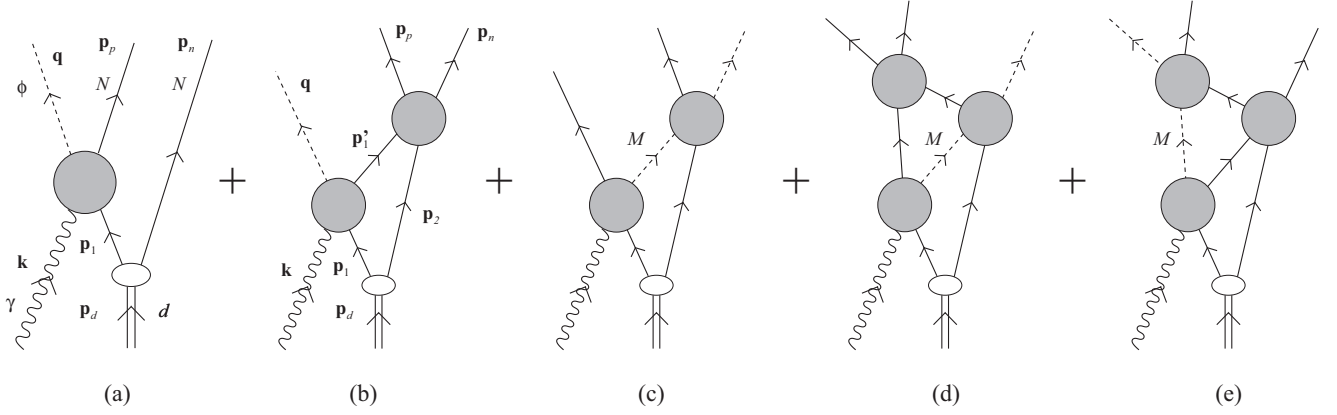


FIG. 2. The diagrams of the $\gamma d \rightarrow \phi pn$ reaction up to triple scatterings. Here meson $M = \pi, \eta, \rho, \omega, \phi, \dots$. Panel (a) is the single-scattering diagram, (b) the double-scattering diagram with FSI between the final nucleons, (c) the double-scattering diagram with FSI between meson and final nucleon, and (d),(e) the triple-scattering diagrams. In this work we consider only the contributions from diagrams (a)–(c), namely, up to double scatterings.

denoted by m and the naming follows that of the momenta. Because the Pomeron amplitude contains spin-spin- and spin-orbital-dependent terms, which are responsible for the spin-flip transition at forward angles and affect the angular distribution of $\phi \rightarrow K^+ K^-$, we include the D state of the deuteron in our calculation.

It is important to note that Eq. (10) explicitly implies that the deuteron is treated nonrelativistically in our study. It has the consequence that the intermediate nucleons with three-momenta \mathbf{p}_1 and \mathbf{p}_2 in Fig. 1 are both on the mass shell and the energy in the intermediate states is not conserved, namely, $E_1(\mathbf{p}_1) + E_2(\mathbf{p}_2) \neq E_d$, where $E_i(\mathbf{p}_i) = (M^2 + \mathbf{p}_i^2)^{1/2}$. This point is brought up often in the subsequent discussion.

In this study, the deuteron wave function Φ_d , including that of the D state, as prescribed from the Bonn potential [23], is employed.

1. Single-scattering amplitudes

The diagram for a single-scattering amplitude from a deuteron target with no FSI is shown in Fig. 2(a). We have, for the amplitude in which the ϕ meson is produced from one of the nucleons in the deuteron, say, a proton,

$$\begin{aligned} \mathcal{M}_{\gamma pn}^{(s,p)}(\mathbf{k}, \mathbf{p}_1, \mathbf{p}_2, m_\gamma, m_1, m_2; \mathbf{q}, \mathbf{p}_p, \mathbf{p}_n, m_\phi, m_p, m_n) \\ = (2\pi)^3 2E_2 \delta^{(3)}(\mathbf{p}_n - \mathbf{p}_2) \delta_{m_n m_2} \\ \times \mathcal{M}_{\gamma p}(\mathbf{k}, \mathbf{p}_1, m_\gamma, m_1; \mathbf{q}, \mathbf{p}_p, m_\phi, m_p), \end{aligned} \quad (11)$$

where the superscripts s and p refer to the fact that the amplitude arises from single scattering in which the ϕ meson is produced on a proton target.

The amplitude $\mathcal{M}_{\gamma p}$ in Eq. (11) denotes the $\gamma p \rightarrow \phi p$ elementary amplitude with the spins and momenta of the particles specified within the parentheses. It should be noted that this is not the one obtained from the Feynman rules in which the four-momenta are conserved. This is because we treat deuterons nonrelativistically so that the struck proton is on the mass shell. Accordingly, only the three-momentum in the subprocess $\gamma p \rightarrow \phi p$ would be conserved but not the

energy, namely, the energies of the initial state $E_\gamma(\mathbf{k}) + E_p(\mathbf{p}_1)$ and the final state $E_\phi(\mathbf{q}) + E_p(\mathbf{p}_p)$ do not have to be equal.

In this work, we adopt the following recipe to obtain $\mathcal{M}_{\gamma\phi}$ in Eq. (11). We start from the corresponding invariant amplitudes $\mathcal{M}_{\gamma\phi}$ with $t = (q - k)^2$ and $s = (q + p_p)^2$ as given in Eqs. (A2) and (A7) for the Pomeron- and (π, η) -exchange amplitudes \mathcal{M}_P and $\mathcal{M}_{\pi+\eta}$ of Appendix A as well as the resonance amplitude outlined there and then express them in terms of the respective momenta and spin variables of all four particles of γ, ϕ and the incoming and outgoing nucleons in the c.m. frame. We first transform the four-momenta of the particles in the initial (final) state to the c.m. frames of the initial (final) state. Here we have $E_\gamma^{c.m.}(\mathbf{p}_i^{c.m.}) + E_p^{c.m.}(-\mathbf{p}_i^{c.m.})$ and $E_\phi^{c.m.}(\mathbf{p}_f^{c.m.}) + E_p^{c.m.}(-\mathbf{p}_f^{c.m.})$ as the initial and final total energies in the c.m. frame, respectively. We then take an approximation where, using the notation $\mathbf{p}_i^{c.m.} = (|\mathbf{p}_i^{c.m.}|, \Omega_i^{c.m.})$, the initial momentum magnitude $|\mathbf{p}_i^{c.m.}|$ is chosen such that the resulting initial total energy would be equal to that of the final. Notice that the direction of the momentum $\Omega_i^{c.m.}$ is kept constant. It is reasonable to do this because the actual energy of the system is the energy of ϕN in the final state. The spins of the particles are also, in general, different after the Lorentz transformation. They are transformed by using the proper transformation for each spin. The photon and ϕ -meson polarization wave functions are transformed by using the ordinary Lorentz transformation for four momenta, while the spinor of the nucleon is transformed by using the Lorentz transformation for spin- $\frac{1}{2}$ spinor.

To obtain the contribution of the ϕ production produced from proton in the deuteron via single scattering to \mathcal{M}_{fi} , the amplitude $\mathcal{M}_{\gamma pn}^{(s,p)}$ of Eq. (11) should be convoluted with the deuteron wave function as in Eq. (10).

The amplitude in which the ϕ meson is produced on the neutron can be written similarly as Eq. (11) with some suitable changes.

2. Double-scattering amplitudes

The double-scattering diagram in which the outgoing proton and neutron rescatter is shown in Fig. 2(b) and the

corresponding amplitude can be expressed as, neglecting the spins,

$$\begin{aligned} \mathcal{M}_{\gamma pn}^{(d)}(\mathbf{k}, \mathbf{p}_1, \mathbf{p}_2; \mathbf{q}, \mathbf{p}_p, \mathbf{p}_n) \\ = \bar{u}(\mathbf{p}_p)\bar{u}(\mathbf{p}_n)\hat{M}_{NN}u(\mathbf{p}_2)\frac{(\not{p}'_1 + m)}{p_1'^2 - m^2 + i\epsilon} \\ \times \epsilon_\mu^*(\mathbf{q})\hat{M}_{\gamma\phi}^{\mu\nu}u(\mathbf{p}_1)\epsilon_\nu(\mathbf{k}), \end{aligned} \quad (12)$$

in which the superscript d denotes that the amplitude arises from double-scattering process. Here \hat{M}_{NN} and $\hat{M}_{\gamma\phi}^{\mu\nu}$ are related to the invariant amplitude \mathcal{M} by the relations

$$\mathcal{M}_{NN} = \bar{u}(\mathbf{p}_3)\bar{u}(\mathbf{p}_4)\hat{M}_{NN}u(\mathbf{p}_1)u(\mathbf{p}_2) \quad (13)$$

for the reaction $N(\mathbf{p}_1) + N(\mathbf{p}_2) \rightarrow N(\mathbf{p}_3) + N(\mathbf{p}_4)$ and

$$\mathcal{M}_{\gamma\phi} = \epsilon_\mu^*(\mathbf{q})\bar{u}(\mathbf{p}')\hat{M}_{\gamma\phi}^{\mu\nu}u(\mathbf{p})\epsilon_\nu(\mathbf{k}), \quad (14)$$

for the reaction $\gamma(\mathbf{k}) + N(\mathbf{p}) \rightarrow \phi(\mathbf{q}) + N(\mathbf{p}')$.

As mentioned earlier, the nucleons in the deuteron with three-momentum \mathbf{p}_i in Fig. 2(b) are treated as on the mass shell and hence would propagate only forward. So, only the positive-energy component in the Feynman propagator

$$S_F(p'_1) = \frac{(\not{p}'_1 + m)}{p_1'^2 - m^2 + i\epsilon} \quad (15)$$

for the nucleon intermediate states with four-momentum p'_1 in Eq. (12) would be kept. It is then a straightforward exercise to arrive at the expression

$$\begin{aligned} \mathcal{M}_{\gamma pn}^{(d,+)}(\mathbf{k}, \mathbf{p}_1, \mathbf{p}_2; \mathbf{q}, \mathbf{p}_p, \mathbf{p}_n) \\ = \frac{1}{2E'_1} \frac{\mathcal{M}_{NN}(NN \rightarrow NN)\mathcal{M}_{\gamma\phi}(\gamma N \rightarrow \phi N)}{E - (E_\phi + E'_1 + E_2) + i\epsilon}, \end{aligned} \quad (16)$$

where superscript $+$ denotes that only positive-energy intermediate states are retained and, $\mathbf{p}'_1 = \mathbf{k} + \mathbf{p}_1 - \mathbf{q}$, $E'_1 = (M^2 + \mathbf{p}_1^2)^{1/2}$, and $E = E_\phi + E_p + E_n$. It has to be noticed that in Eq. (16), summation over intermediate spins is understood.

Again, both $\mathcal{M}_{NN}(NN \rightarrow NN)$ and $\mathcal{M}_{\gamma\phi}(\gamma N \rightarrow \phi N)$ in the above Eq. (16); only the three-momentum is conserved but not necessarily the energy. We already encountered this problem for $\mathcal{M}_{\gamma\phi}(\gamma N \rightarrow \phi N)$ when discussing the case of single scattering and the same recipe is followed. For $\mathcal{M}_{NN}(NN \rightarrow NN)$, we note that it is what is called the t -matrix element in the potential scattering and is given by $t = v + v g_0 t$. In addition, the propagator in Eq. (16) contains two parts,

$$\begin{aligned} \frac{1}{E - (E_\phi + E'_1 + E_2) + i\epsilon} \\ = \mathcal{P} \frac{1}{E - (E_\phi + E'_1 + E_2)} - i\pi\delta[E - (E_\phi + E'_1 + E_2)]. \end{aligned} \quad (17)$$

The first and second terms on the right-hand side would correspond to the half-off- and on-energy-shell rescatterings between the final pn states, respectively. The half-off-shell and the on-shell $\mathcal{M}_{NN}(NN \rightarrow NN)$ matrix elements are hence needed. We evaluate them with the Nijmegen potential [19,20].

Equation (16) has to be convoluted with the deuteron wave function as the case of single scattering.

Another type of double-rescattering diagram involves intermediate mesons like π , η , ρ , ω , and ϕ first produced by the photon as depicted in Fig. 2(c), can also be treated in a manner similar to that in Fig. 2(b), as outlined above. However, it can be estimated to be small as follows. We realize that the total cross sections $\sigma(i)$ arising from an intermediate state i are roughly proportional to the product of the cross sections of its intermediate reactions:

$$\begin{aligned} \sigma(NN) &\propto \sigma_{\gamma N \rightarrow \phi N} \sigma_{NN \rightarrow NN}, \\ \sigma(\phi N) &\propto \sigma_{\gamma N \rightarrow \phi N} \sigma_{\phi N \rightarrow \phi N}, \\ \sigma(\pi N) &\propto \sigma_{\gamma N \rightarrow \pi N} \sigma_{\pi N \rightarrow \phi N}. \end{aligned} \quad (18)$$

Now the values for the total cross sections of the intermediate reactions relevant to the kinematic region with photon LAB energy $E_\gamma \sim 2$ GeV are [24,25]

$$\begin{aligned} \sigma_{\gamma N \rightarrow \phi N} &\approx 0.3 \mu\text{b}, \\ \sigma_{\gamma N \rightarrow \pi N} &\approx 5 \mu\text{b}, \\ \sigma_{NN \rightarrow NN} &\approx 10^6 \mu\text{b}, \\ \sigma_{\phi N \rightarrow \phi N} &\approx 11 \times 10^3 \mu\text{b}, \\ \sigma_{\pi N \rightarrow \phi N} &\approx 30 \mu\text{b}, \end{aligned} \quad (19)$$

which give

$$\begin{aligned} \sigma(NN) &\propto 3 \times 10^5, \\ \sigma(\phi N) &\propto 3.3 \times 10^3, \\ \sigma(\pi N) &\propto 1.5 \times 10^2, \end{aligned} \quad (20)$$

or

$$\sigma(NN) : \sigma(\phi N) : \sigma(\pi N) = 1 : 1.1 \times 10^{-2} : 5 \times 10^{-4}. \quad (21)$$

For the cross sections whose values are not available, like $\sigma(\rho N)$ and $\sigma(\omega N)$, it is likely that their values are of the same order of magnitude as that of $\sigma(\pi N)$, as π , ρ , and ω are all meson with zero strangeness. For $\sigma(\eta N)$, its value is probably close to that of $\sigma(\phi N)$, because η , like ϕ , contains $s\bar{s}$. Because $\sigma(NN)$ is roughly the same order of magnitude as the DCSs arising from a single-scattering process, $\sigma(\phi N)$ and $\sigma(\eta N)$ are then around a few percent of it. It can then be concluded that if the ϕN and ηN intermediate states are incorporated, at most, their contributions are just a few percent of the total cross section. This result is also supported by Ref. [18], where it is shown that the effect arising from the ϕN FSI is small.

III. RESULTS

With the model presented in the preceding section, it is straightforward to calculate the DCSs, SDMEs, and other observables of the $\gamma d \rightarrow \phi pn$ reaction. We remind the readers that once our model for the elementary amplitude of $\gamma p \rightarrow \phi p$ is fixed and the γNN^* couplings determined, as explained briefly in Sec. II B and in detail in Appendix A, our results for $\gamma d \rightarrow \phi pn$ are simply predictions and free from any fitting.

We present the results and focus on the role played by the resonances, the effects of Fermi motion, and the FSI before

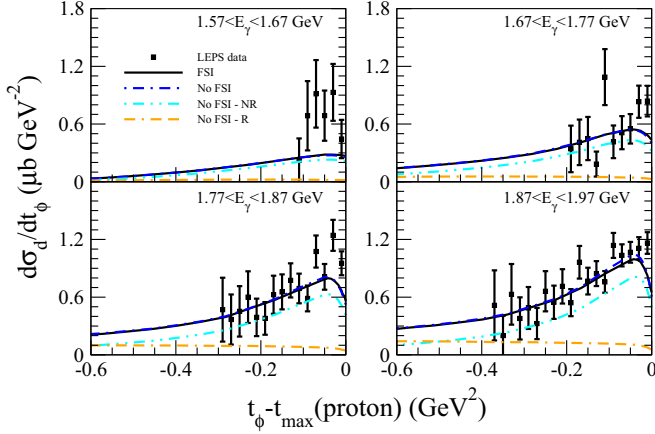


FIG. 3. The DCS of $\gamma d \rightarrow \phi pn$ as a function of t_ϕ at four energy bins: $1.57 < E_\gamma < 1.67$ GeV, $1.67 < E_\gamma < 1.77$ GeV, $1.77 < E_\gamma < 1.87$ GeV, and $1.87 < E_\gamma < 1.97$ GeV. The solid lines are the results of $NR + R$ with pn FSI. The dash-dotted, dash-dot-dotted, and dash-dash-dotted lines are the results of $NR + R$, NR , and R without pn FSI, respectively. Here NR and R denote nonresonant and resonant amplitudes, respectively. The squares with error bars are the experimental data of Refs. [16,26].

comparing them with the existing data, first for the DCS and then for the SDME. In our discussion of the SDMEs, the connections between the spin dependence and the elementary amplitudes, as well as the values of SDMEs, are pointed out.

A. Differential cross sections

The DCSs as functions of t_ϕ at eight energy bins from LEPS [16,26] are given in Figs. 3–6. The DCSs as functions of t_ϕ at $1.65 < E_\gamma < 1.75$ GeV measured by CLAS [17] are shown in Fig. 7. The ratio of the DCSs with only FSI to the DCSs without the FSI at several incoming photon LAB energies is given in Fig. 8. The DCSs at $t_\phi = t_{\max}$ and their ratio to twice of the production from free proton, where t_{\max} corresponds to the value of the maximum t for free proton case [16,26], are

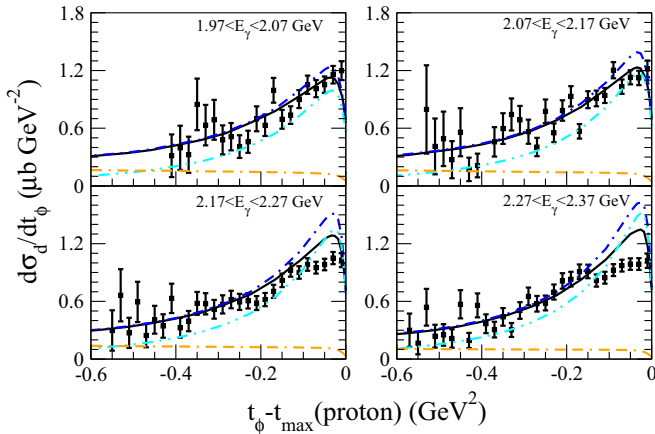


FIG. 4. The same as in Fig. 3, but for four energy bins: $1.97 < E_\gamma < 2.07$ GeV, $2.07 < E_\gamma < 2.17$ GeV, $2.17 < E_\gamma < 2.27$ GeV, and $2.27 < E_\gamma < 2.37$ GeV.

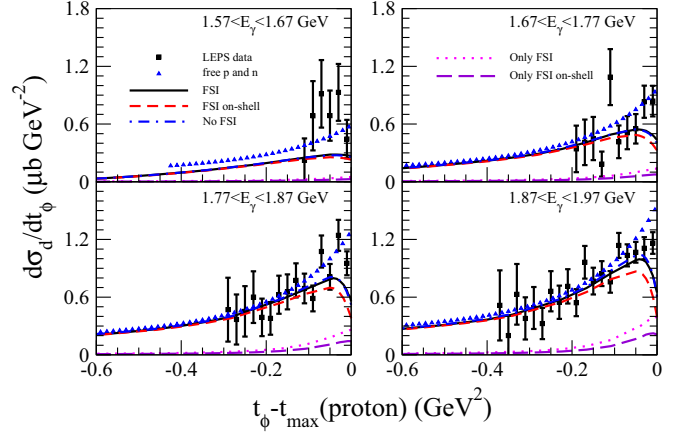


FIG. 5. The DCS of $\gamma d \rightarrow \phi pn$ as a function of t_ϕ at four energy bins: $1.57 < E_\gamma < 1.67$ GeV, $1.67 < E_\gamma < 1.77$ GeV, $1.77 < E_\gamma < 1.87$ GeV, and $1.87 < E_\gamma < 1.97$ GeV. The triangles are the results for the simple summation of free proton and neutron DCSs. The solid, dashed, and dash-dotted lines are the results of $NR + R$ with pn FSI, with only on-shell pn FSI, and without pn FSI, respectively. The dotted and long-dashed lines are the results of $NR + R$ with pn FSI and with only on-shell pn FSI, respectively, without the single-scattering contribution. Here NR and R denote nonresonant and resonant amplitudes, respectively. The squares with error bars are the experimental data of Refs. [16,26].

given in Fig. 9. The ratio of the DCS from the proton inside the deuteron to that of the free proton case as a function of photon LAB energy [16,26] is given in Fig. 10(a).

The solid and dash-dotted lines are the results obtained by including nonresonant and resonant amplitudes with and without pn FSI, respectively. Here including pn FSI means that we include both the on- and the off-shell rescattering effects. The dashed lines are the results obtained by including only the on-shell part of the pn FSI. The dash-dot-dotted and dash-dash-dotted lines are the results without pn FSI calculated by including only nonresonant and resonant amplitudes, respectively. The dotted lines are the results of

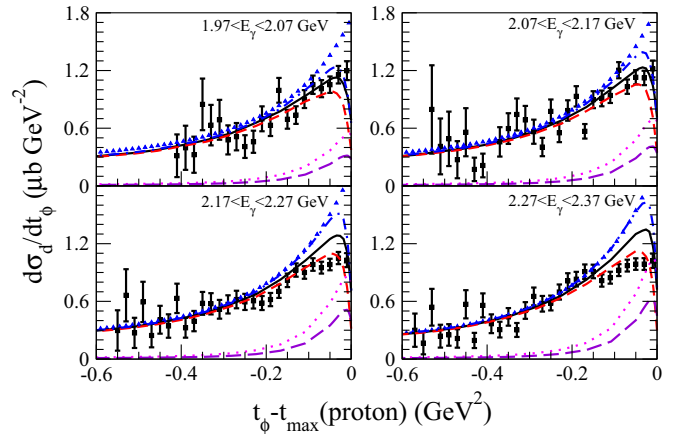


FIG. 6. Caption is the same as in Fig. 5, but for four energy bins: $1.97 < E_\gamma < 2.07$ GeV, $2.07 < E_\gamma < 2.17$ GeV, $2.17 < E_\gamma < 2.27$ GeV, and $2.27 < E_\gamma < 2.37$ GeV.

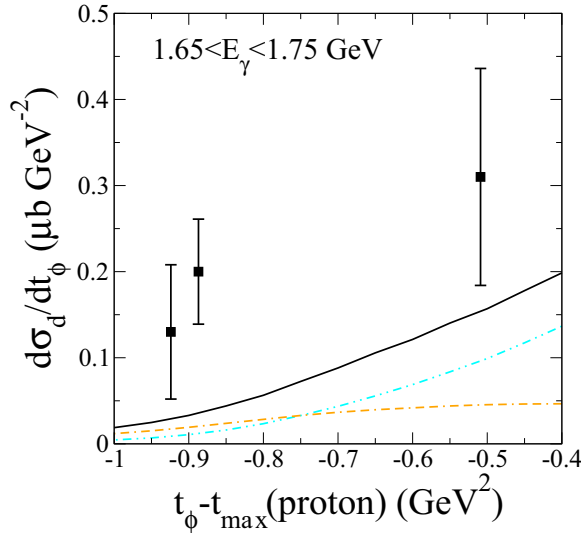


FIG. 7. Comparison of our prediction with CLAS data of Ref. [17] for $1.65 < E_\gamma < 1.75$ GeV. Notation for the curves is the same as in Fig. 3.

nonresonant plus resonant amplitudes with pn FSI without the single-scattering contribution. The long-dashed lines are plotted similarly to the dotted ones, but with only the on-shell part included. Our results are plotted by using the middle values of each bin and the maximum value of t for the free proton case $t_{\max}(\text{proton})$ corresponds to these values as well. The squares with error bars are the LEPS data [15,16,26].

1. The role of the resonance

In Figs. 3 and 4, it is seen that the resonance contribution to the DCS as a function of t , given by dash-dash-dotted lines (orange), is basically flat and small. However, the single-scattering results for DCSs with resonance (dash-dotted lines) are significantly larger than those without resonance (dash-dot-dotted lines). This indicates that the resonant amplitude in

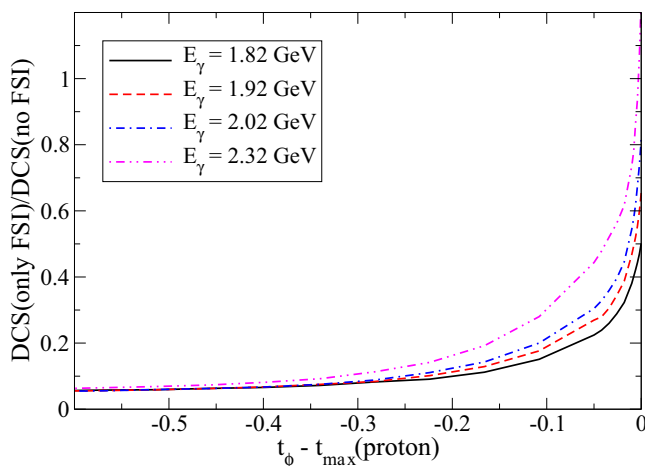


FIG. 8. The ratio of the DCS with only FSI to the DCS without the FSI at several incoming photon LAB energies.

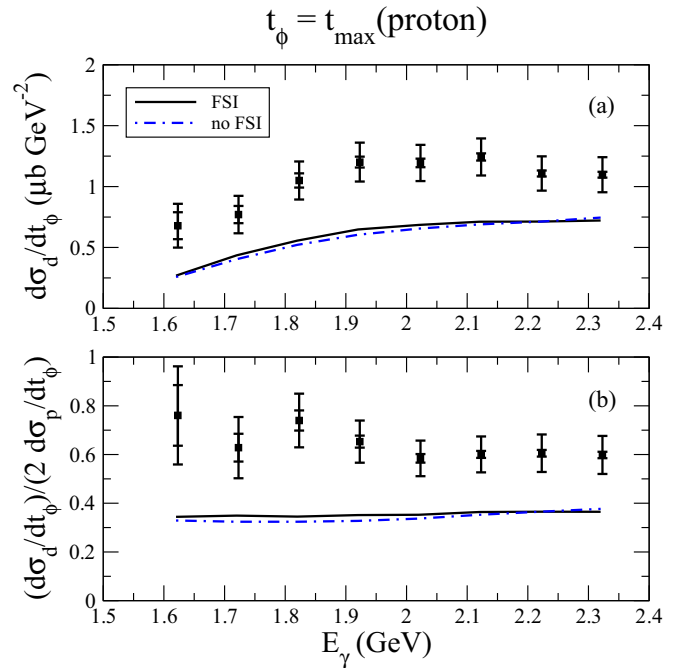


FIG. 9. (a) The DCS of $\gamma d \rightarrow \phi pn$ and (b) the ratio of the DCS of $\gamma d \rightarrow \phi pn$ to twice the DCS of $\gamma p \rightarrow \phi p$, both at $t_\phi = t_{\max}(\text{proton})$ as a function of E_γ . The notation is as in Fig. 3 and the dash-dotted lines are the results with resonance but without pn FSI.

general interferes constructively with the nonresonant amplitude. This is in agreement with our findings in Refs. [13,14]. This feature is also seen in Fig. 7. Here we notice in Figs. 3, 4, and 7 that the single-scattering results for DCSs with resonance (dash-dotted lines) are significantly larger than those without resonance (dash-dot-dotted lines). The effects of the resonance are the most conspicuous at $|t_\phi - t_{\max}(\text{proton})| \sim 0.6$ GeV², where the resonance contribution is about equal to the nonresonant part and is essential to bring our predictions into agreement with the data there, which are available only for energy bins of $2.17 < E_\gamma < 2.27$ GeV and $2.27 < E_\gamma < 2.37$ GeV shown in the bottom panels of Fig. 4.

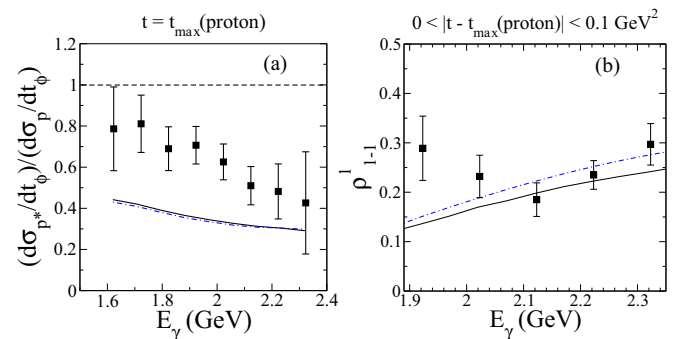


FIG. 10. (a) The ratio of DCS of $\gamma p \rightarrow \phi p$, where the proton is inside the deuteron to that of free proton, and (b) the SDME ρ_{1-1}^1 , both as functions of E_γ . The notation is as in Fig. 9.

2. The effects of Fermi motion

To understand the role of Fermi motion in the reaction, it is instructive to compare the results of the DCS obtained by simple summation of free proton and neutron DCSs (triangles) and those obtained by using deuteron target without the pn FSI (dash-dotted lines) in Figs. 5 and 6. Such a comparison avoids the complication incurred by the presence of the pn FSI. It is easily noted that the results are very different at small momentum transfer $|t_\phi - t_{\max}(\text{proton})|$ and gradually become more similar at larger momentum transfer. This feature is easy to understand. It is obvious that when the momentum transfer to the deuteron is larger than the momentum of the Fermi motion, the effects from the latter would become less important. Clearly, at very large momentum transfer, the outgoing struck nucleon would have an absolute velocity large enough such that its initial absolute velocity arising from Fermi motion would become negligible.

It is also worth mentioning that the results for the DCSs of the free nucleons are always above those of the deuteron case without pn FSI. This is caused by the shape of the energy dependence of the DCS of the $\gamma N \rightarrow \phi N$, which decreases sharply toward low energy, but increases slowly toward high energy. For each value of energy, the Fermi motion will sample this dependence around the energy, and because of the shape of the dependence, the average for the DCSs is weighed toward the low energy, where the change is more drastic, hence its lower values relative to that of the free case. It is also the reason why the differences between the DCSs of the free nucleons and that of the deuteron case are more obvious at lower-energy bins.

Unlike the DCS of the free nucleon case, which goes to zero drastically at $t_\phi = t_{\max}(\text{proton})$, the DCS of the $\gamma d \rightarrow \phi pn$ reaction goes to zero more gradually. This is caused also by the Fermi motion of the nucleons inside the deuteron. The nucleon moving at the opposite direction of the photon provides the reaction the opportunity to produce ϕ meson at momentum transfer t_ϕ smaller than $t_{\max}(\text{proton})$ of the free case.

Naively, without considering the internal structure of the deuteron, as well as the pn FSI, one expects that the DCS of $\gamma d \rightarrow \phi pn$ reaction is just a sum of the DCSs of $\gamma p \rightarrow \phi p$ and $\gamma n \rightarrow \phi n$. Indeed, when the two mechanisms affect only minimally, for example, at higher energy and larger momentum transfer t_ϕ , as one sees from Figs. 5 and 6, the results from $\gamma d \rightarrow \phi pn$ are very close to that obtained by summing the DCSs of $\gamma p \rightarrow \phi p$ and $\gamma n \rightarrow \phi n$.

3. The effects of FSI

In Fig. 3, it is seen that the differences between results with FSIs (solid lines) and the one without the inclusion of FSIs (dash-dotted lines) are rather small in the photon energy range of 1.57–1.97 GeV. However, the difference becomes conspicuous in the region $|t_\phi - t_{\max}(\text{proton})| \leq 0.2 \text{ GeV}^2$ as the photon energy grows larger than 1.97 GeV, as seen in Fig. 4. Besides the fact that FSI effects grow with photon energy, a close look further reveals that FSI effects also increase as $|t_\phi - t_{\max}(\text{proton})|$ decreases, as depicted in Fig. 8, which gives the ratio of DCS (only FSI)/DCS (no FSI) for the four energy bins in Figs. 3 and 4.

The two distinct features of the FSI effects, as mentioned in the above, namely, that they grow with increasing photon energy and decreasing $|t_\phi - t_{\max}(\text{proton})|$ are related to the fact that the pn cross section drops quickly with increasing energy [27]. The reason that FSI effects get magnified with smaller values of $|t_\phi - t_{\max}(\text{proton})|$ is simply because the invariant mass M_{pn} of pn is monotonically decreasing with $|t_\phi - t_{\max}(\text{proton})|$. With a smaller M_{pn} , the available c.m. energy for the pn system, or equivalently the relative kinetic energy in the c.m. system of outgoing pn pair also gets smaller such that their interaction becomes stronger. The growing FSI effects with increasing photon energy can be understood in the same light by noting that the difference between $|t_{\max}(\text{deuteron})|$ and $|t_{\max}(\text{proton})|$ becomes smaller in the mean time, as pointed out in Ref. [18].

Another important and interesting feature of the FSI effect is that the inclusion of the final pn rescattering, in general, brings down the DCS. One first notes that the pn FSI actually consists of two parts, the on- and off-shell parts of the integrals over the pn intermediate states, as indicated in Eq. (17). It can be shown that the DCS obtained by taking into account only the on-shell part of the pn FSI is actually equal to the DCS arising from the single-scattering interactions [Fig. 2(a)] minus the DCS arising from exclusively the on-shell part of the pn FSI [Fig. 2(b)]. This interesting result can be understood theoretically as a consequence of the unitarity of the $pn \rightarrow pn$ amplitude and is independent of the details of the interaction. The proof is given in Appendix C. At $E_\gamma \sim 2 \text{ GeV}$ and $|t_\phi - t_{\max}(\text{proton})| < 0.05 \text{ GeV}^2$, the DCSs with on-shell pn FSI (dashed), shown in Figs. 5 and 6, are around 40% lower than the results without the pn FSI. The large on-shell pn FSI effects contradicts the results of Ref. [18], where it is found to be small. This can be understood as a consequence of the fact that their $\gamma d \rightarrow \phi pn$ and $pn \rightarrow pn$ amplitudes are not unitary. This suggests that unitarity of the reactions taking place in the final state should be taken into account in a study that includes FSIs.

The inclusion of the off-shell FSI brings up the DCSs again, as seen in Figs. 5 and 6; namely, the effects of on-shell and off-shell FSI cancel out each other to some extent. In the end, the total pn FSI results (solid lines), in general, lie between the results with only on-shell FSI included (red dashed lines) and those without pn FSI (blue dash-dotted lines). For example, at $E_\gamma \sim 2 \text{ GeV}$ and $|t_\phi - t_{\max}(\text{proton})| < 0.05 \text{ GeV}^2$, the final DCSs are only around 20% lower than the results without pn FSI, after both the on-shell and the off-shell FSI are considered. This demonstrates that the off-shell FSIs are important as they actually reduce the effects introduced by the on-shell ones up to about 50% at these kinematics.

4. Comparison with the data

We next compare our results for the DCSs with the LEPS data [16,26]. Here, in Figs. 3 and 4, our results without both resonance and pn FSI, as given by the dash-dot-dotted line, show a strong peaking tendency at small values of $|t_\phi - t_{\max}(\text{proton})|$, especially at higher energies, as indicated by the data. However, they are, in general, smaller than the data, except at the peak region of $|t_\phi - t_{\max}(\text{proton})| < 0.05 \text{ GeV}^2$ at the highest-energy bin of $2.27 < E_\gamma < 2.37 \text{ GeV}$ considered

in this study. After the inclusion of the resonance contribution, but not pn FSI effects, the results (dash-dotted line) are all shifted by roughly the same amount for all $|t_\phi - t_{\max}(\text{proton})|$. The inclusion of the resonance improves the agreement with data at lower energies but overshoots the data at small values of $|t_\phi - t_{\max}(\text{proton})| < 0.05 \text{ GeV}^2$ at higher energies. Last, when the pn FSI is included in addition to the resonance, the agreement with the data improves as the FSI significantly reduces the peak.

Nevertheless, some discrepancies remain at small momentum transfer, namely, in the peak region, especially at photon energies higher than 2.17 GeV, where at the highest-energy bin, a difference of about 25% is observed. However, our prediction for the peak in the lowest-energy bin $1.57 < E_\gamma < 1.67 \text{ GeV}$ is considerably lower than the data. In the end, with all the effects included, our DCS results underestimate the data at lower energies while overestimating them at higher energies. Notice also that our DCS results explain the LEPS data well at larger momentum transfer but not at small momentum transfer. However, when comparing with the CLAS data of Ref. [17], which is taken at a large momentum transfer of $-0.9 < t_\phi - t_{\max}(\text{proton}) < -0.5 \text{ GeV}^2$ in the energy bin of $1.65 < E_\gamma < 1.75 \text{ GeV}$, as shown in Fig. 7, we find that our predictions are lower than the data.

It is to be noted that at t_ϕ very close to $t_{\max}(\text{proton})$, the LEPS data do not fall to zero, while our results do. It is suggested by the main author [26] of Ref. [16] that it is possible that, owing to the binning size of the data, the sharp decrease of the DCS around $t_\phi = t_{\max}(\text{proton})$ might not have been represented well in the experimental results.

The comparison of our results for the $d\sigma_d/dt_\phi$ and $(d\sigma_d/dt_\phi)/(2d\sigma_p/dt_\phi)$ at forward direction $t_\phi = t_{\max}(\text{proton})$ to the data of Ref. [16] is presented in Fig. 9. In Fig. 10(a), we also compare our results of the ratio of $(d\sigma_{p^*}/dt_\phi)/(d\sigma_p/dt_\phi)$ to the data of Ref. [16], where $d\sigma_{p^*}/dt_\phi$ is the DCS of $\gamma p \rightarrow \phi p$ in which the ϕ meson is produced from the proton inside the deuteron. Here we observe that our results do not match the data, even though the shapes are generally in agreement with the data. As these results are taken in the forward direction, it is possible that the problem is related to the size of the bins as discussed above. Last, it is important to point out here that in both the data and our results, no clear peak corresponding to the resonance shows up in Fig. 9(a). This is readily understandable as the resonance is weak and easily gets smeared out by the Fermi motion and FSI with the deuterium target.

B. Spin-density matrix elements

The SDMEs as functions of t_ϕ from LEPS at three energy bins [15] are shown in Figs. 11–13, and the SDMEs ρ_{1-1}^1 as functions of photon LAB energy are presented in Fig. 10(b). The notation is the same as in Figs. 3–5. Namely, solid, dashed-dotted, and dash-dot-dotted lines denote results obtained with resonance and FSI included, only resonance but no FSI included, and without both resonance and FSI included, respectively. We first elaborate on the role of the spin dependence of the elementary amplitude, as well as the roles of resonance and FSI, before discussing the comparison with data.

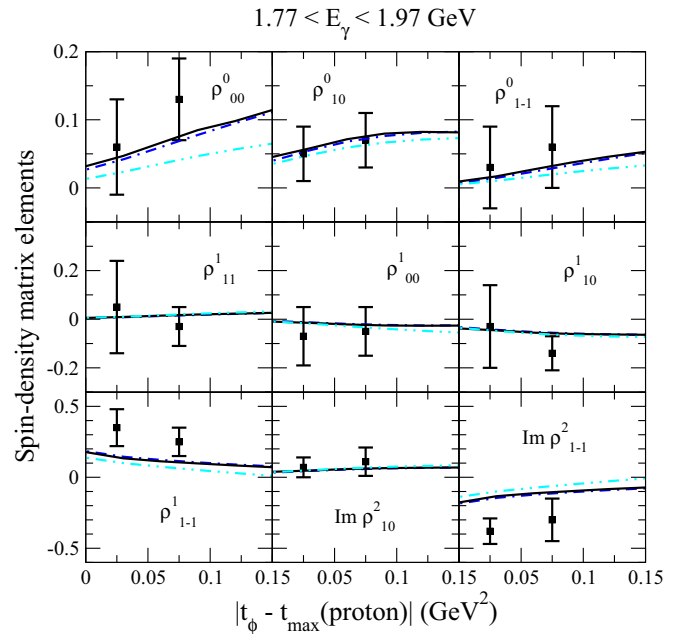


FIG. 11. The results for the SDME of $\gamma d \rightarrow \phi pn$ reaction for $1.77 < E_\gamma < 1.97 \text{ GeV}$ with resonance and pn FSI, with resonance but without pn FSI, and without both resonance and pn FSI are given by solid, dash-dotted, and dash-dot-dotted lines, respectively. The data are from Ref. [15].

1. The spin dependence of the elementary amplitude of $\gamma N \rightarrow \phi N$

The proper spin dependence of the elementary $\gamma N \rightarrow \phi N$ amplitude is employed in our calculation, whereas its dependence on the nucleon spin was simply neglected in Ref. [18]. Without the use of such spin dependence, it is not

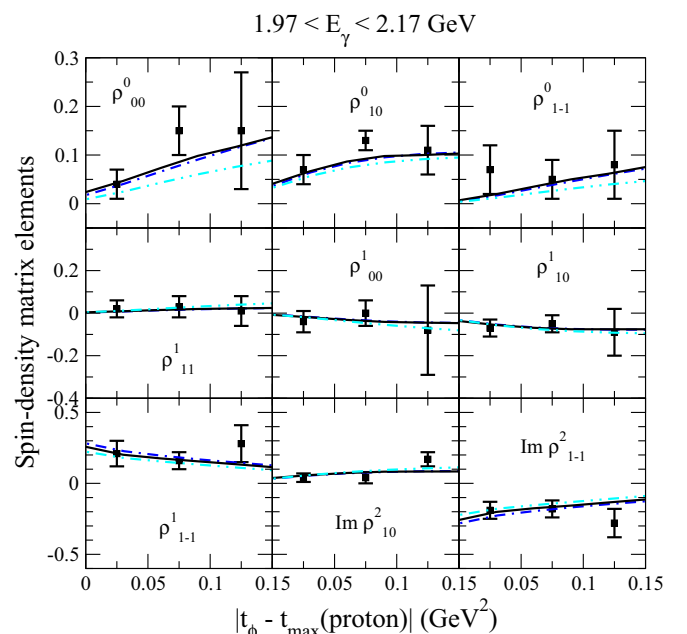


FIG. 12. The same as in Fig. 11, but for $1.97 < E_\gamma < 2.17 \text{ GeV}$.

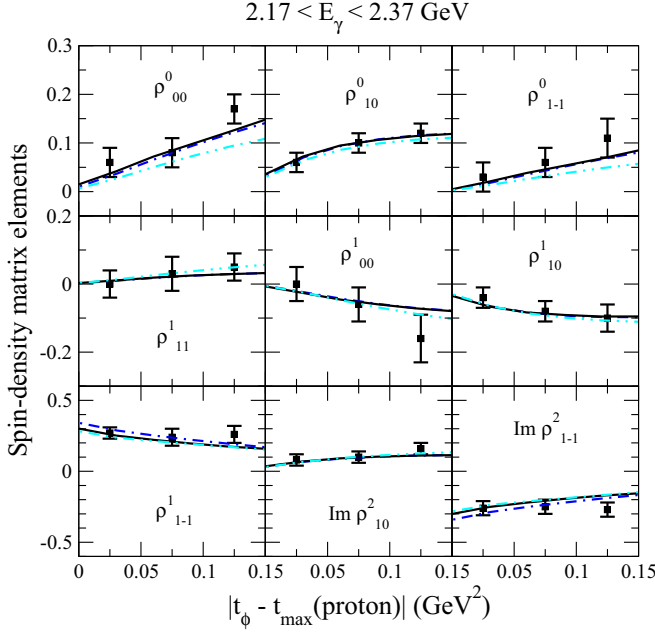


FIG. 13. The same as in Fig. 11, but for $2.17 < E_\gamma < 2.37$ GeV.

possible to describe the SDME data because all of them would be zero except for $\rho_{1-1}^1 = -\text{Im}\rho_{1-1}^2 = 0.5$.

2. The role of the resonance

For the SDMEs, we observe in Figs. 11–13 that the inclusion of the resonance does not affect as much as in the case of DCSs, as seen in the difference between dashed-dotted, and dash-dot-dotted lines, except the ρ_{00}^0 . This means that it does not change much the polarization properties of the reaction. This is a consequence of the normalization of the SDMEs being proportional to the DCS. However, in terms of percentage, the ρ_{1-1}^0 , ρ_{11}^1 , ρ_{1-1}^1 , and $\text{Im}\rho_{1-1}^2$ elements are all rather significantly changed, especially at larger momentum transfer, in agreement with what we found in Ref. [14].

The enhancement of the ρ_{00}^0 element results from the increase on the production of the ϕ meson of helicity $\lambda_\phi = 0$. However, the enhancement of the ρ_{11}^1 and ρ_{1-1}^1 elements indicates that double-spin-flip transition with $\lambda_\phi = -\lambda_\gamma$ increases. This is actually a consequence of the fact that the resonance process is not helicity conserving, in contrast to the Pomeron-exchange process, which is basically helicity conserving. The enhancement of the ρ_{1-1}^1 and $\text{Im}\rho_{1-1}^2$ elements basically shows that the resonance does increase the natural-parity production which is already strongly reduced by the π - and η -exchange processes.

It is important to note that, even for the elements where the resonance does not seem to affect much, it is misleading to think that it does not contribute. As explained in Ref. [14], the resonance does contribute; however, the interference between resonance and nonresonance processes somewhat balances the resonance contribution in the opposite direction.

3. The effects of FSI

In Figs. 11–13, it is observed that the solid and dash-dotted lines almost sit on each other, which implies that the FSI effects on the SDME are minimal, even at the highest-energy bin, $2.17 < E_\gamma < 2.37$ GeV, where the FSI effect on the DCS has been substantial. This is a consequence of the fact that the SDMEs are actually normalized by the amplitude square. It also reflects the fact that the final pn rescattering does not change the spin distribution of the produced ϕ meson.

The only two SDMEs significantly changed by the pn FSI are ρ_{1-1}^1 and $\text{Im}\rho_{1-1}^2$ at small $|t_\phi - t_{\text{max}}(\text{proton})|$ values. The reductions from this effect are around 15% in the highest-energy bin. This basically shows that the pn FSI actually increases the strength of the unnatural-parity exchange mediated by the intermediate π and η relative to that of natural-parity exchange by the Pomeron. This can be understood readily. First, consider the case without the pn FSI. Here, notice that the strength of the unnatural-parity exchange in the incoherent case would be lower than the free proton one because in the former, the final proton and neutron moving at similar velocities would cause their π -exchange amplitudes to interfere destructively. However, the pn FSI decreases the production of the final proton and neutron moving at similar velocities, which enhances the strength of unnatural-parity exchange and manifests in the smaller values of the two SDMEs mentioned in the above.

Finally, it is also interesting to note that the reduction on ρ_{1-1}^1 and $\text{Im}\rho_{1-1}^2$ owing to rescattering of final pn is not caused by stronger double-spin-flip transition where $\lambda_\phi = -\lambda_\gamma$ in which λ_γ (λ_ϕ) is the helicity of photon (ϕ meson) although these two SDMEs contain contributions from this transition. It can be seen from Figs. 11–13 in which the SDMEs ρ_{1-1}^0 and ρ_{11}^1 , which are measures of the strength of the double-spin-flip transition, basically almost vanish at small $|t_\phi - t_{\text{max}}(\text{proton})|$ values.

4. Comparison with the data

We observe that the presence of the resonance helps improve the agreement with data for ρ_{00}^0 at all energies. However, the resonance does not help the description of ρ_{1-1}^1 and $\text{Im}\rho_{1-1}^2$ at the lowest-energy bin $1.77 < E_\gamma < 1.97$ GeV. As for the inclusion of the pn FSI, we observe that it does not bring any significant betterment to the agreement of our results with the data. After including all the effects, we notice that the description of ρ_{1-1}^1 and $\text{Im}\rho_{1-1}^2$ at the lowest-energy bin, $1.77 < E_\gamma < 1.97$ GeV, is still off from the data. Similarly, our results for the energy dependence of ρ_{1-1}^1 at small momentum transfer of $|t_\phi - t_{\text{max}}(\text{proton})| < 0.1$ GeV² in Fig. 10(b) describe the data well, but poorly at lower energies. This indicates that the data favors more contribution from natural-parity exchange which is usually provided by Pomeron exchange.

C. Discussions

From the comparisons between our predictions with the data as presented in Secs. III A 4 and III B 4, it is seen that the

overall agreement is satisfactory; namely, the main features of the data are all properly reproduced except for a few quantitative discrepancies.

Regarding the DCS, the most serious discrepancies between the data and our results lie in the neighborhood of the forward direction, i.e., small values of $|t_\phi - t_{\max}(\text{proton})|$, as seen in Figs. 3 and 4. One notices that the height of the predicted peak is at first underpredicted at the lower-energy bins with the difference getting smaller with increasing energy and then eventually overshoots the data. Yet at the very forward direction with $t_\phi = t_{\max}(\text{proton})$, our predictions are always smaller than the data, as seen in Fig. 9(a). It might be related to the binning size of the data [26], as discussed in Sec. III A 4. For the intermediate momentum-transfer region with $0.2 < |t_\phi - t_{\max}(\text{proton})| < 0.5 \text{ GeV}^2$, our results describe well the data. However, as momentum transfer grows and becomes larger than $0.5 < |t_\phi - t_{\max}(\text{proton})| \text{ GeV}^2$, our results underestimate the CLAS data of Ref. [17], as indicated in Fig. 7. However, it should be noted that these data are taken at a rather low-energy bin of $1.65 < E_\gamma < 1.75 \text{ GeV}$ among the data set we consider in this study.

The SDMEs measured by LEPS are, in general, reproduced well by our calculations besides ρ_{1-1}^1 and $\text{Im}\rho_{1-1}^2$ in the low-energy bin of $1.77 < E_\gamma < 1.97 \text{ GeV}$. This happens to be the case in our model for the elementary amplitude of $\gamma p \rightarrow \phi p$ [14].

The discrepancies summarized above are characterized by (i) very low energies for all momentum transfers and (ii) forward angles except for the energy bins lying between 1.87 and 2.17 GeV.

It is then an interesting question to ask why our model, which has performed well in the $\gamma p \rightarrow \phi p$ case, does not describe $\gamma d \rightarrow \phi pn$ as well as one would expect despite that we have treated the problem laboriously up to the double-scattering contributions. The higher-order multiple rescatterings as depicted in Figs. 2(d) and 2(e) are likely not to be blamed because they all involve at least one meson-nucleon scattering and hence would not contribute significantly, as discussed in Sec. II C 2. The only possibility left then is the model we employ for the elementary process $\gamma N \rightarrow \phi N$. This is also supported by noting that the disagreement found in the SDMEs is somewhat similar to that in the free proton case presented in Ref. [14].

Three possible causes have come to our mind. Namely, (i) description of the resonance, (ii) off-shell behavior of the elementary amplitude, and (iii) low-energy behavior of the model.

Discussing the role of the resonance in $\gamma d \rightarrow \phi pn$ reaction, one first notes that to study the $\gamma d \rightarrow \phi pn$ reaction, a model for the $\gamma n \rightarrow \phi n$ reaction is required. The background part of the Pomeron, π , and η exchanges can be readily obtained with isospin invariance. Regarding the resonance contribution, there is a problem in that there exist no data for ϕ production from the neutron to infer the couplings of $\gamma n N^*$ and $\phi n N^*$ such that we have to rely on some model assumptions for estimation. However, we find from Figs. 3 and 4 that the resonance contribution is rather independent of momentum transfer, as in the case of $\gamma p \rightarrow \phi p$ [14], while discrepancies appear to be the largest at small momentum transfer. Accordingly, an improved

description of the resonance may not be sufficient to bridge the discrepancy. Nevertheless, it has to be remembered that resonance does play a significant role in reducing the difference with the data, especially for the DCS and some elements of the SDME at larger momentum transfer. Another interesting question concerns whether some peak feature would appear in $\gamma d \rightarrow \phi pn$, as in $\gamma p \rightarrow \phi p$. In this connection, it is to be remembered that, according to our analysis in Ref. [14], the nonmonotonic behavior found in Ref. [10] is a result of a subtle balance between the meson-exchange mechanism and a weak resonance. Such a balance could easily be offset by the Fermi motion and FSI in the ϕ production from deuteron.

In Figs. 5 and 6 it can be observed that our DCS results with resonance and on-shell rescattering only (dashed lines) fit the data very well at higher energies, though not as well at lower energies. This may be related to the possibility that the off-shell rescattering contribution to the DCS is not satisfactorily estimated. This is indeed an open question as the Pomeron amplitude itself, which constitutes the largest contribution to the DCS, is not yet fully understood, not to mention its off-energy-shell behavior as is needed in our calculation. This question should be investigated in more detail.

The low-energy behavior of our model, basically that of the Pomeron amplitude, as well as contributions from other mechanisms like the existence of a second Pomeron, glueball exchange, and $s\bar{s}$ knockout, etc., has been the subject of several studies, e.g., Refs. [6,28]. Again, they remain to be studied in depth.

The issues enumerated above could possibly be answered by the recent high-statistics data on the $\gamma p \rightarrow \phi p$ DCSs and SDMEs taken at CLAS [11,12]. Their DCS data, taken at a larger range of momentum transfer and energy, also confirm the nonmonotonic behavior observed at small momentum transfer previously by LEPS. However, their data indicate that the nonmonotonic behavior does not appear at larger momentum transfer. This, in fact, could possibly cast some doubts on whether the nonmonotonic behavior is really caused by the presence of a resonance. We have recently realized that the $s\bar{s}$ knockout mechanism, as considered in Ref. [8], could also produce nonmonotonic behavior in the forward differential cross section of $\gamma p \rightarrow \phi p$ and are currently engaged in an attempt to extend our model for $\gamma p \rightarrow \phi p$ [14] by including the $s\bar{s}$ knockout process to see whether it is possible to explain the LEPS data [10,15] and the recent CLAS data [11,12]. It will conceivably shed useful light on the issues discussed above.

IV. SUMMARY AND CONCLUSIONS

In summary, we have calculated the DCSs and SDMEs of the incoherent photoproduction of ϕ meson from deuteron $\gamma d \rightarrow \phi pn$ near threshold and compared them with the data from the LEPS [15,16] and CLAS [17]. The calculation is based on a model for $\gamma p \rightarrow \phi p$ we constructed in Refs. [13,14] which described the LEPS data of Ref. [10] well, including a peak around a photon laboratory energy of 2.0 GeV, first observed by the LEPS Collaboration and recently confirmed by the high-statistics CLAS data [11,12]. Our model contains a resonance with spin-parity $J^P = 3/2^-$, mass $M_{N^*} = 2.08 \pm$

0.04 GeV, and width $\Gamma_{N^*} = 0.570 \pm 0.159$, in addition to a background consisting of Pomeron and (π, η) exchanges in the t channel. For production from deuteron, the couplings of the resonance to neutron are estimated with a guide from a relativistic constituent quark model. The calculation for $\gamma d \rightarrow \phi pn$ was then carried out up to double rescatterings with realistic nucleon-nucleon interaction.

Our calculation contains major improvements over that of Ref. [18] in that (i) the Pomeron amplitude used is more realistic and contains the proper spin dependence, which leads to nontrivial values for the SDME, (ii) the D state of deuteron is considered, and (iii) the off-shell contributions to the FSI of the final pn , in addition to the on-shell part, are included. Accordingly, our results are, up to double rescatterings, predictions of the $\gamma d \rightarrow \phi pn$ reaction because no more fitting is involved.

We find that the inclusion of the Fermi motion of the nucleons inside the deuteron plays an important role in the description of one characteristic of $\gamma d \rightarrow \phi pn$ at small momentum transfer, namely, a gradual decrease of DCSs with diminishing $|t_\phi - t_{\max}(\text{proton})|$. However, the contribution from deuteron D state to both DCSs and SDMEs is negligible.

The effects of FSI involving meson-nucleon rescatterings are estimated to be small. However, the effects from the rescattering of the final pn are found to be rather significant to provide a considerable reduction in the DCS which is about 20% at higher-energy bins. We find that the contributions of on-shell and off-shell final pn rescatterings cancel each other out to some extent. The off-shell rescattering effects should hence be considered in realistic description of the reaction. It brings up the question about the off-shell extrapolation of the Pomeron amplitude, an issue that remains to be studied further.

Regarding the postulated resonance, it is found to play a significant role in the description of the DCSs at a broad range of momentum transfer and energy, although less so for the SDMEs. The weak resonance, which is responsible for the appearance of a small peak in $\gamma p \rightarrow \phi p$, is not found to produce any nonmonotonic behavior in $\gamma d \rightarrow \phi pn$, apparently smeared out by the Fermi motion and FSI.

The overall agreement of our results with the data is satisfactory in that the main features of the data are all properly reproduced except a few quantitative discrepancies at some kinematic regions characterized by (i) very low energies at all momentum transfers, and (ii) forward angles except at the energy bins lying between 1.87 and 2.17 GeV.

On the experimental side, the DCS data from LEPS do not fall to zero at small t as would be expected. According to Ref. [26], it might be related to the binning size of the data. It is possible that some aspects of their results might need to be further examined. In addition, the LEPS data have relatively large error bars because they had to rely on MC simulation to separate the coherent and incoherent events. The comparison of our predictions with the data will be more meaningful after these questions are clarified.

On the theoretical side, our model for the elementary amplitude of $\gamma p \rightarrow \phi p$ should be carefully compared with the recent high-statistics data from CLAS [11,12], especially regarding the assumption of resonance. Other possible mechanisms like nondiffractive processes of nucleon exchange,

nucleon resonances, second Pomeron exchange, t -channel scalar meson and glueball exchanges, and $s\bar{s}$ -cluster knockout, which have been suggested to contribute at low energies, should also be reexamined, in light of the new CLAS data. We recently realized that the $s\bar{s}$ knockout mechanism as studied in Ref. [8] could also produce nonmonotonic behavior in the forward differential cross section of $\gamma p \rightarrow \phi p$ and are currently engaged in an attempt to extend our model for $\gamma p \rightarrow \phi p$ [14] by including the $s\bar{s}$ knockout process to see whether it is possible to account for the LEPS data [10,15] and the recent high-statistics CLAS data [11,12]. Finally, we emphasize that a combined analysis of the low-energy data of $\gamma p \rightarrow \phi p$ and $\gamma d \rightarrow \phi pn$ will be much desired to shed light on the issues discussed above.

ACKNOWLEDGMENTS

We would like to thank Dr. Wen Chen Chang for useful discussions and correspondences. This work was supported in parts by National Science Council of the Republic of China (Taiwan) under Grant No. NSC100-2112-M002-012. We would also like to acknowledge the help from National Taiwan University High-Performance Computing Center in providing us with a fast and dependable computation environment, which is essential in carrying out this work. A.K. would like to thank IHEP, Beijing, Center of Theoretical Science, National Taiwan University, and National Center for Theoretical Sciences, Hsin-Chu, Taiwan, for support for visits to the respective institutions during the course of this study. Y.B.D. also thanks the Sino-German CRC 110 ‘‘Symmetries and the Emergence of Structure in QCD’’ project (NSFC Grant No. 11261130311) and the Center of Theoretical Sciences, National Taiwan University for their hospitalities.

APPENDIX A: THE MODEL FOR $\gamma N \rightarrow \phi N$ REACTION

We first introduce the kinematic variables k , p_i , q , and p_f for the four-momenta of the incoming photon, initial proton, outgoing ϕ -meson, and final proton, respectively, with $s = (k + p_i)^2 = (q + p_f)^2$, $t = (q - k)^2 = (p_f - p_i)^2$, and $u = (p_f - k)^2 = (q - p_i)^2$.

In addition to the nonresonant mechanism of Pomeron exchange, t -channel π - and η -exchange, we include a resonance N^* . We can then write the full amplitude \mathcal{M} as

$$\mathcal{M}_{\gamma N \rightarrow \phi N} = \mathcal{M}_P + \mathcal{M}_{\pi+\eta} + \mathcal{M}_{N^*}, \quad (\text{A1})$$

as shown in Fig. 14, where \mathcal{M}_{N^*} contains both s - and u -channel contributions.

1. Pomeron exchange

Following Refs. [6,29], we can easily write the Pomeron-exchange amplitude of Fig. 14(a),

$$\begin{aligned} \mathcal{M}_P &= -\bar{u}(p_f, \lambda_{N'}) M(s, t) \Gamma^{\mu\nu} u(p_i, \lambda_N) \\ &\quad \times \varepsilon_\mu^*(q, \lambda_\phi) \varepsilon_\nu(k, \lambda_\gamma), \end{aligned} \quad (\text{A2})$$

where $\varepsilon_\mu(q, \lambda_\phi)$ and $\varepsilon_\nu(k, \lambda_\gamma)$ are the polarization vectors of the ϕ meson and photon with λ_ϕ and λ_γ , respectively, and $u(p_i, \lambda_N)$ [$\bar{u}(p_f, \lambda_{N'})$] is the Dirac spinor of the nucleon with

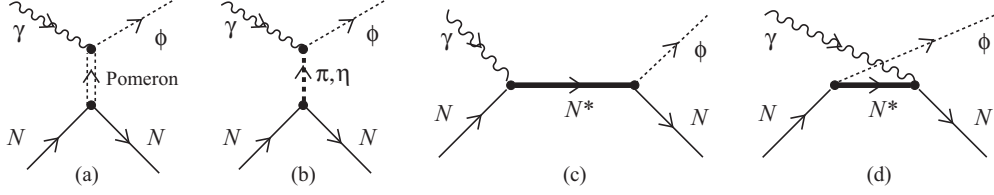


FIG. 14. Pomeron, (π, η) exchanges, and s - and u -channel N^* excitation diagrams for $\gamma N \rightarrow \phi N$ reaction are labeled (a)–(d), respectively.

momentum p_i [p_f] and helicity λ_N [$\lambda_{N'}$]. The transition operator $\Gamma^{\mu\nu}$ in Eq. (A2) is

$$\Gamma^{\mu\nu} = \left(g^{\mu\nu} - \frac{q^\mu q^\nu}{q^2} \right) \not{k} - \left(k^\mu - \frac{kq q^\mu}{q^2} \right) \gamma^\nu - \left(\gamma^\mu - \frac{q q^\mu}{q^2} \right) \left[\not{q}^\nu - \frac{kq(p_i^\nu + p_f^\nu)}{k(p_i + p_f)} \right]. \quad (\text{A3})$$

The scalar function $M(s, t)$ is described by the Reggeon parametrization,

$$M(s, t) = C_P F_1(t) F_2(t) \frac{1}{s} \left(\frac{s - s_{th}}{s_0} \right)^{\alpha_P(t)} \exp \left[-\frac{i\pi}{2} \alpha_P(t) \right], \quad (\text{A4})$$

where we have taken the Pomeron trajectory $\alpha_P(t) = 1.08 + 0.25t$ and $s_0 = (M_N + M_\phi)^2$. The isoscalar form factor $F_1(t)$ of the nucleon and the form factor $F_2(t)$ of the ϕ -photon–Pomeron coupling are given as [2,6]

$$F_1(t) = \frac{4M_N^2 - a_N^2 t}{(4M_N^2 - t)(1 - t/t_0)^2}, \quad (\text{A5})$$

$$F_2(t) = \frac{2\mu_0^2}{(1 - t/M_\phi^2)(2\mu_0^2 + M_\phi^2 - t)}, \quad (\text{A6})$$

with $\mu_0^2 = 1.1 \text{ GeV}^2$, $a_N^2 = 2.8$, and $t_0 = 0.7 \text{ GeV}^2$.

Here the strength factor is taken to be $C_P = 3.65$, which is obtained by fitting to the total cross-section data at high energy [6]. Included as well is the threshold factor s_{th} [3,6] so that we get a better agreement with experimental data near the threshold region. Owing to the fact that Pomeron properties and behaviors at lower energies are not well established, we adjust this parameter to fit the experimental data on the DCSs around $E_\gamma = 6 \text{ GeV}$ because at this energy, it can be expected that all other contributions from hadronic intermediate states would become negligible and only Pomeron contributes. Also, around this energy, experimental data have relatively small error bars and rise steadily without much fluctuation. These give us confidence to match the Pomeron contribution to the experimental data at this energy by fixing $s_{th} = 1.3 \text{ GeV}^2$.

2. π - and η -meson exchanges

The amplitudes for the π and η exchanges in the t channel [Fig. 14(b)] can be calculated straightforwardly [8] and are given by

$$\mathcal{M}_{\pi+\eta} = \frac{-e g_{\gamma\phi\pi} g_{\pi NN} F_\pi^2(t)}{M_\phi} \bar{u}(p_f, \lambda_{N'}) \gamma_5 \frac{\varepsilon^{\mu\nu\rho\sigma} q_\mu k_\rho}{t - M_\pi^2} \times u(p_i, \lambda_N) \varepsilon_\nu^*(q, \lambda_\phi) \varepsilon_\sigma(k, \lambda_\gamma)$$

$$+ \frac{e g_{\gamma\phi\eta} g_{\eta NN} F_\eta^2(t)}{M_\phi} \bar{u}(p_f, \lambda_{N'}) \gamma_5 \frac{\varepsilon^{\mu\nu\rho\sigma} q_\mu k_\rho}{t - M_\eta^2} \times u(p_i, \lambda_N) \varepsilon_\nu^*(q, \lambda_\phi) \varepsilon_\sigma(k, \lambda_\gamma), \quad (\text{A7})$$

with the coupling constants $g_{\pi NN} = 13.26$, $g_{\gamma\phi\pi} = -0.14$, and $g_{\gamma\phi\eta} = -0.71$, as well as the form factors $F_\pi(t)$ and $F_\eta(t)$ for the virtually exchanged mesons at the MNN and $\gamma\phi M$ ($M = \pi, \eta$) vertices, respectively, are taken to be the same as in Ref. [29]. We choose $g_{\eta NN} = 1.12$ [30] and $\Lambda_\pi = \Lambda_\eta = 1.2 \text{ GeV}$, which are slightly different with the values given in Ref. [29].

3. Excitation of a baryon resonance

The s - and u -channel Feynman diagrams with an N^* in the intermediate state are shown in Figs. 14(c) and 14(d). For the coupling of $3/2$ resonances to γN , we choose the commonly used interaction Lagrangians [30–32]

$$\mathcal{L}_{\gamma NN^*}^{3/2^\pm} = i e g_{\gamma NN^*}^{(1)} \bar{\psi}_N \Gamma^\pm (\partial^\mu \psi_{N^*}^\nu) \tilde{F}_{\mu\nu} + e g_{\gamma NN^*}^{(2)} \bar{\psi}_N \Gamma^\pm \gamma^5 (\partial^\mu \psi_{N^*}^\nu) F_{\mu\nu} + \text{H.c.}, \quad (\text{A8})$$

where $F_{\mu\nu} = \partial_\mu A_\nu - \partial_\nu A_\mu$ is the electromagnetic field tensor, and $\sigma_{\mu\nu} = \frac{i}{2}(\gamma_\mu \gamma_\nu - \gamma_\nu \gamma_\mu)$. Also, $\tilde{F}_{\mu\nu} = \frac{1}{2} \epsilon_{\mu\nu\alpha\beta} F^{\alpha\beta}$ denotes the dual electromagnetic field tensor with $\epsilon^{0123} = +1$. The operators Γ^\pm are given by $\Gamma^+ = 1$ and $\Gamma^- = \gamma_5$. For the ϕNN^* interaction Lagrangians, we have

$$\mathcal{L}_{\phi NN^*}^{3/2^\pm} = i g_{\phi NN^*}^{(1)} \bar{\psi}_N \Gamma^\pm (\partial^\mu \psi_{N^*}^\nu) \tilde{G}_{\mu\nu} + g_{\phi NN^*}^{(2)} \bar{\psi}_N \Gamma^\pm \gamma^5 (\partial^\mu \psi_{N^*}^\nu) G_{\mu\nu} + i g_{\phi NN^*}^{(3)} \bar{\psi}_N \Gamma^\pm \gamma^5 \gamma_\alpha (\partial^\alpha \psi_{N^*}^\nu - \partial^\nu \psi_{N^*}^\alpha) (\partial^\mu G_{\mu\nu}) + \text{H.c.}, \quad (\text{A9})$$

where $G^{\mu\nu}$ is defined as $G^{\mu\nu} = \partial^\mu \phi^\nu - \partial^\nu \phi^\mu$, with ϕ^μ the field of ϕ meson. The dual field tensor $\tilde{G}_{\mu\nu}$ is defined similarly as its electromagnetic counterpart with $F^{\alpha\beta} \rightarrow G^{\alpha\beta}$. Notice that we could have chosen to describe the γNN^* in the same way as we describe the ϕNN^* interactions. However, the term proportional to $g_{\gamma NN^*}^{(3)}$ in the Lagrangian densities of Eq. (A9) vanishes in the case of a real photon. With the Lagrangians given in Eqs. (A8) and (A9), the full invariant amplitude of s and u channels can be obtained by following the Feynman rules.

The form factor for the vertices used in the s - and u -channel diagrams, $F_{N^*}(p^2)$, is

$$F_{N^*}(p^2) = \frac{\Lambda^4}{\Lambda^4 + (p^2 - M_{N^*}^2)^2}, \quad (\text{A10})$$

where Λ is the cutoff parameter for the virtual N^* , following Ref. [33]. In this work, we choose $\Lambda = 1.2$ GeV for all resonances. The Rarita-Schwinger propagator is used for the spin- $\frac{3}{2}$ N^* ,

$$G_{\mu\nu}^{(3/2)}(p) = \frac{i(\not{p} + M_{N^*})}{p^2 - M_{N^*}^2 + iM_{N^*}\Gamma_{N^*}} \left[-g_{\mu\nu} + \frac{1}{3}\gamma_\mu\gamma_\nu - \frac{1}{3M_{N^*}}(p_\mu\gamma_\nu - p_\nu\gamma_\mu) + \frac{2}{3M_{N^*}^2}p_\mu p_\nu \right], \quad (\text{A11})$$

with Γ_{N^*} the total decay width of N^* . Because $u < 0$, we take $\Gamma_{N^*} = 0$ MeV for the propagator in the u channel.

Note carefully that in our previous works [13,14], we cannot obtain the values of the coupling constants $g_{\phi pp^*}$ and $g_{\gamma pp^*}$ by fitting to the experimental data, as our calculations are done in the tree level. Thus, only the values of the products of the coupling constants $G_{\gamma pp^*}^{ij} \equiv g_{\gamma pp^*}^{(i)}g_{\phi pp^*}^{(j)}$ are shown. Here we show how we calculate the neutron-coupling constants $g_{\phi nn^*}^{(j)}$ and $g_{\gamma nn^*}^{(i)}$.

First of all, we have to realize that we do not have sufficient knowledge to actually estimate the neutron-coupling constants $g_{\phi nn^*}^{(j)}$ and $g_{\gamma nn^*}^{(i)}$ from the experimental data. At best, we can only assume that our resonance, if it actually exists, should have properties rather similar to a theoretically predicted $J^P = 3/2^-$ nucleon state in the same mass region that has the same sign for the ratio of helicity amplitudes $A_{1/2}^p/A_{3/2}^p$ for $p^* \rightarrow \gamma p$. For this purpose, we employ a $J^P = 3/2^-$ nucleon state with a bare mass of 2095 GeV and a positive value for the ratio of helicity amplitudes $A_{1/2}^p/A_{3/2}^p$ for γp decay predicted by Ref. [21] in which the predictions for Breit-frame helicity amplitudes $A_{1/2}^N$ and $A_{3/2}^N$ for both γp and γn decays are

$$\begin{aligned} A_{1/2}^p &= -9, & A_{3/2}^p &= -14, \\ A_{1/2}^n &= 8, & A_{3/2}^n &= 1, \end{aligned} \quad (\text{A12})$$

in the unit of $10^{-3}\text{GeV}^{-1/2}$. Notice that these helicity amplitudes are calculated in Breit frame, not in the center-of-mass frame. It is also very interesting to note that this predicted state is the only nucleon state with $J^P = 3/2^-$ and a positive ratio of helicity amplitudes $A_{1/2}^p/A_{3/2}^p$ in the energy region.

Let us also state the relation between the helicity and invariant amplitudes in the center-of-mass frame of the resonance N^* ,

$$A_m^N = \frac{1}{\sqrt{2|\mathbf{k}|}} \frac{1}{\sqrt{2M_{N^*}}} \frac{1}{\sqrt{2M_N}} \mathcal{M}_{N^* \rightarrow \gamma N}(m, m_\gamma = +1), \quad (\text{A13})$$

where \mathbf{k} is the three-momentum of the photon in center-of-mass frame and $m = 1/2, \dots, J$ is the spin projection of the resonance in which J is the total spin of the resonance. The

photon is assumed to be moving to the positive z direction with spin projection $m_\gamma = +1$.

By using the values for the helicity amplitudes $A_{1/2}^n$ and $A_{3/2}^n$ for the $n^* \rightarrow \gamma n$, it is straightforward to calculate the coupling constants $g_{\gamma nn^*}$. First, let us translate the coupling constants into helicity amplitudes by using a linear transformation, because they are related only linearly,

$$\begin{pmatrix} A_{1/2}^N \\ A_{3/2}^N \end{pmatrix} = \begin{pmatrix} \Lambda_{11} & \Lambda_{12} \\ \Lambda_{21} & \Lambda_{22} \end{pmatrix} \begin{pmatrix} g_{\gamma NN^*}^{(1)} \\ g_{\gamma NN^*}^{(2)} \end{pmatrix}, \quad (\text{A14})$$

where

$$\Lambda_{ij} = A_{i-1/2}^N \Big|_{g_{\gamma NN^*}^{(j)}=1, g_{\gamma NN^*}^{(\neq j)}=0}, \quad (\text{A15})$$

where m and m_γ are the spin projections of the resonance N^* and the photon, respectively. Here $N = (p, n)$ and $N^* = (p^*, n^*)$. It must also be noted that because the helicity amplitudes are defined for real photon, there is no $m_\gamma = 0$ with $m_N = +1/2$ state for the $A_{1/2}^N$ amplitude. Finally, to obtain $g_{\gamma nn^*}^{(i)}$, we can just inverse the relation

$$\begin{pmatrix} g_{\gamma nn^*}^{(1)} \\ g_{\gamma nn^*}^{(2)} \end{pmatrix} = \begin{pmatrix} \Lambda_{11} & \Lambda_{12} \\ \Lambda_{21} & \Lambda_{22} \end{pmatrix}^{-1} \begin{pmatrix} A_{1/2}^n \\ A_{3/2}^n \end{pmatrix}. \quad (\text{A16})$$

Next we calculate the coupling constants $g_{\phi nn^*}^{(j)}$. Notice that by isospin consideration, the values for these coupling constants are the same for both proton and neutron cases $g_{\phi pp^*}^{(j)} = g_{\phi nn^*}^{(j)}$. First of all, we notice that we only have the products of $G_{\gamma pp^*}^{ij} \equiv g_{\gamma pp^*}^{(i)}g_{\phi pp^*}^{(j)}$ in our previous work [14], and the values of $g_{\gamma pp^*}^{(i)}$ here cannot be similar to those obtained in Ref. [21], as they are obtained in completely different ways. However, we have to find a way to obtain $g_{\gamma pp^*}^{(i)}$ if we would like to get $g_{\phi pp^*}^{(j)}$ from $G_{\gamma pp^*}^{ij}$. However, we can require that the resonance in our work and in Ref. [21] should have the same decay width to γp to fix $g_{\gamma pp^*}^{(i)}$. Let us also write the partial width of the nucleon resonance N^* decay into γN in terms of the helicity amplitudes,

$$\Gamma_{N^* \rightarrow \gamma N} = \frac{2}{2J+1} \frac{|\mathbf{k}|^2 M_N}{\pi^2 M_{N^*}} (|A_{1/2}^N|^2 + |A_{3/2}^N|^2). \quad (\text{A17})$$

Then the $p^* \rightarrow \gamma p$ width in Ref. [21] is

$$\Gamma_{p^* \rightarrow \gamma p} = f_A (|A_{1/2}^p|^2 + |A_{3/2}^p|^2), \quad (\text{A18})$$

in which f_A , which can be easily read from Eq. (A17), is just a factor containing kinematical variables. At the same time, as we explained before, this width has to be equal to the width we have from the coupling constants $g_{\gamma pp^*}^{(i)}$,

$$\begin{aligned} \Gamma_{p^* \rightarrow \gamma p} &= f_g^{(1)} (g_{\gamma pp^*}^{(1)})^2 + f_g^{(2)} (g_{\gamma pp^*}^{(2)})^2 \\ &= f_g^{(1)} (g_{\gamma pp^*}^{(1)})^2 + f_g^{(2)} (k_{12} g_{\gamma pp^*}^{(1)})^2 \\ &= (f_g^{(1)} + f_g^{(2)} k_{12}^2) (g_{\gamma pp^*}^{(1)})^2, \end{aligned} \quad (\text{A19})$$

where $k_{12} \equiv g_{\gamma pp^*}^{(2)}/g_{\gamma pp^*}^{(1)} = G_{\gamma pp^*}^{2j}/G_{\gamma pp^*}^{1j}$ and $f_g^{(i)}$ is just a factor containing kinematical variables. This leads us to

$$g_{\gamma pp^*}^{(1)} = \pm \sqrt{\frac{f_A}{f_g^{(1)} + f_g^{(2)}k_{12}^2}} \sqrt{|A_{1/2}^p|^2 + |A_{3/2}^p|^2},$$

$$g_{\gamma pp^*}^{(2)} = \pm k_{12} \sqrt{\frac{f_A}{f_g^{(1)} + f_g^{(2)}k_{12}^2}} \sqrt{|A_{1/2}^p|^2 + |A_{3/2}^p|^2}, \quad (\text{A20})$$

which can be written compactly as

$$g_{\gamma pp^*}^{(i)} = \pm k_{1i} \sqrt{\frac{f_A}{f_g^{(1)} + f_g^{(2)}k_{12}^2}} \sqrt{|A_{1/2}^p|^2 + |A_{3/2}^p|^2}, \quad (\text{A21})$$

where $k_{11} = 1$. Notice that the ambiguity in the sign can be resolved easily by substituting the coupling constants to Eq. (A14) and requiring the resulting helicity amplitudes to have the same sign as the ones given in Ref. [21]. Once we obtain $g_{\gamma pp^*}^{(i)}$, we can also obtain $g_{\phi pp^*}^{(j)} = g_{\phi NN^*}^{(j)}$,

$$g_{\phi NN^*}^{(j)} = \frac{G_{\gamma pp^*}^{ij}}{g_{\gamma pp^*}^{(i)}} = \sqrt{\frac{f_g^{(1)} + f_g^{(2)}k_{12}^2}{f_A}} \times \frac{G_{\gamma pp^*}^{ij}}{k_{1i} \sqrt{|A_{1/2}^p|^2 + |A_{3/2}^p|^2}}. \quad (\text{A22})$$

APPENDIX B: SPIN-DENSITY MATRIX FORMALISM FOR $\gamma d \rightarrow \phi pn$ REACTION

Let us begin by defining the SDME from the decay angular distribution of the $K\bar{K}$ pair in an arbitrary frame for a specific t and photon polarization state [34] $|\gamma\rangle$,

$$W(\Omega_{K\bar{K}})|_{t_\phi} = \frac{1}{N} \int du_\phi d\Omega_{pn} \frac{P_{pn}}{M_{pn}} \times \sum_{\lambda_p \lambda_n \lambda_d} |\langle \Omega_{K\bar{K}} \lambda_p \lambda_n | \hat{T} | \gamma \lambda_d \rangle|^2, \quad (\text{B1})$$

with a normalization factor

$$N = \frac{1}{2} \int d\Omega_{K\bar{K}} \int du_\phi d\Omega_{pn} \frac{P_{pn}}{M_{pn}} \times \sum_{\lambda_p \lambda_n \lambda_\gamma \lambda_d} |\langle \Omega_{K\bar{K}} \lambda_p \lambda_n | \hat{T} | \lambda_\gamma \lambda_d \rangle|^2, \quad (\text{B2})$$

where all the kinematic variables have been defined before in Sec. II, except the solid angle $\Omega_{K\bar{K}}$, which is the direction of either K or \bar{K} in $K\bar{K}$ pair rest frame. Here λ_i denotes the helicity of particle i . Notice that the integrations over u and Ω_{pn} are needed because we do not observe these variables in the final state. The normalization factor N is proportional with the unpolarized DCS, with a factor of 1/2 needed to average over the helicity states of the photon and an integration over $\Omega_{K\bar{K}}$ is also included. Clearly, the integration has to be done in the same way we would integrate for DCSs because it is

proportional to the decay angular distribution. Here we have dropped all the momenta, and it is understood that the momenta of the particles have been fixed by the total energy squared s , t_ϕ , u_ϕ , Ω_{pn} , and $\Omega_{K\bar{K}}$ together with the use of a coordinate system.

At this point, let us now introduce the photon spin-density operator

$$\hat{\rho}(\gamma) = |\gamma\rangle\langle\gamma|, \quad (\text{B3})$$

which can be represented by a matrix whose elements are

$$\rho_{\lambda_\gamma \lambda'_\gamma}(\gamma) = \langle \lambda_\gamma | \hat{\rho}(\gamma) | \lambda'_\gamma \rangle. \quad (\text{B4})$$

Then we can write Eq. (B1) as

$$W(\Omega_{K\bar{K}})|_{t_\phi} = \frac{1}{N} \int du_\phi d\Omega_{pn} \frac{P_{pn}}{M_{pn}} \sum_{\lambda_p \lambda_n \lambda_d \lambda_\gamma \lambda'_\gamma} \langle \Omega_{K\bar{K}} \lambda_p \lambda_n | \times \hat{T} | \lambda_\gamma \lambda_d \rangle \rho_{\lambda_\gamma \lambda'_\gamma}(\gamma) \langle \lambda'_\gamma \lambda_d | \hat{T}^\dagger | \Omega_{K\bar{K}} \lambda_p \lambda_n \rangle, \quad (\text{B5})$$

with a normalization factor, written in a different way,

$$N = \int d\Omega_{K\bar{K}} \int du_\phi d\Omega_{pn} \frac{P_{pn}}{M_{pn}} \sum_{\lambda_p \lambda_n \lambda_d \lambda_\gamma \lambda'_\gamma} \langle \Omega_{K\bar{K}} \lambda_p \lambda_n | \hat{T} | \lambda_\gamma \lambda_d \rangle \left(\frac{1}{2} \delta_{\lambda_\gamma \lambda'_\gamma} \right) \times \langle \lambda'_\gamma \lambda_d | \hat{T}^\dagger | \Omega_{K\bar{K}} \lambda_p \lambda_n \rangle, \quad (\text{B6})$$

which shows its similarity with the numerator, with an integration over $\Omega_{K\bar{K}}$ and $\rho_{\lambda_\gamma \lambda'_\gamma}(\gamma) \rightarrow 1/2 \delta_{\lambda_\gamma \lambda'_\gamma}$, where $\delta_{\lambda_\gamma \lambda'_\gamma}$ here is the Kronecker δ .

Here by following the same construction, we can write the decay angular distribution as a function of the ϕ -meson SDME,

$$W(\Omega_{K\bar{K}})|_{t_\phi} = \frac{1}{N_\phi} \sum_{\lambda_\phi \lambda'_\phi} \langle \Omega_{K\bar{K}} | \hat{T}_\phi | \lambda_\phi \rangle \rho_{\lambda_\phi \lambda'_\phi}(\phi) \langle \lambda'_\phi | \hat{T}_\phi^\dagger | \Omega_{K\bar{K}} \rangle, \quad (\text{B7})$$

where the normalization constant is

$$N_\phi = \int d\Omega_{K\bar{K}} \sum_{\lambda_\phi \lambda'_\phi} \langle \Omega_{K\bar{K}} | \hat{T}_\phi | \lambda_\phi \rangle \left(\frac{1}{3} \delta_{\lambda_\phi \lambda'_\phi} \right) \langle \lambda'_\phi | \hat{T}_\phi^\dagger | \Omega_{K\bar{K}} \rangle = \frac{1}{3} \sum_{\lambda_\phi} \int d\Omega_{K\bar{K}} |\langle \Omega_{K\bar{K}} | \hat{T}_\phi | \lambda_\phi \rangle|^2, \quad (\text{B8})$$

where the factor of 1/3 comes from the averaging of the polarization of the ϕ meson. Now our main task is to isolate $\rho_{\lambda_\phi \lambda'_\phi}(\phi)$ from Eq. (B5). We can begin by noticing that

$$\langle \Omega_{K\bar{K}} \lambda_p \lambda_n | \hat{T} | \lambda_\gamma \lambda_d \rangle = c \sum_{\lambda_\phi} \langle \Omega_{K\bar{K}} | \hat{T}_\phi | \lambda_\phi \rangle \langle \lambda_\phi \lambda_p \lambda_n | \hat{T}_{\gamma d} | \lambda_\gamma \lambda_d \rangle, \quad (\text{B9})$$

where a complex number c is produced as we take only the pole of the ϕ -meson propagator, which is a good approximation because the ϕ meson has very small width.

After some arranging of the terms, Eq. (B5) can now be written as

$$W(\Omega_{K\bar{K}})|_{t_\phi} = \frac{1}{N} \sum_{\lambda_\phi \lambda'_\phi} \langle \Omega_{K\bar{K}} | \hat{T}_\phi | \lambda_\phi \rangle \left[|c|^2 \sum_{\lambda_p \lambda_n \lambda_d} \sum_{\lambda_\gamma \lambda'_\gamma} \int du_\phi d\Omega_{pn} \frac{P_{pn}}{M_{pn}} \langle \lambda_\phi \lambda_p \lambda_n | \hat{T}_{\gamma d} | \lambda_\gamma \lambda_d \rangle \rho_{\lambda_\gamma \lambda'_\gamma}(\gamma) \langle \lambda'_\gamma \lambda_d | \hat{T}_{\gamma d}^\dagger | \lambda'_\phi \lambda_p \lambda_n \rangle \right] \times \langle \lambda'_\phi | \hat{T}_\phi^\dagger | \Omega_{K\bar{K}} \rangle. \quad (\text{B10})$$

Now let us evaluate the normalization constant,

$$N = \frac{1}{2} \int d\Omega_{K\bar{K}} \int du_\phi d\Omega_{pn} \frac{P_{pn}}{M_{pn}} |c|^2 \sum_{\lambda_p \lambda_n \lambda_\gamma \lambda_d} |\langle \Omega_{K\bar{K}} | \lambda_p \lambda_n | \hat{T} | \lambda_\gamma \lambda_d \rangle|^2 \\ = \frac{1}{2} \int du_\phi d\Omega_{pn} \frac{P_{pn}}{M_{pn}} |c|^2 \sum_{\lambda_\phi \lambda_p \lambda_n \lambda_\gamma \lambda_d} \int d\Omega_{K\bar{K}} |\langle \Omega_{K\bar{K}} | \hat{T}_\phi | \lambda_\phi \rangle|^2 |\langle \lambda_\phi \lambda_p \lambda_n | \hat{T}_{\gamma d} | \lambda_\gamma \lambda_d \rangle|^2. \quad (\text{B11})$$

We can now use the fact that the K meson is a spinless particle, which allows us to write

$$\langle \Omega_{K\bar{K}} | \hat{T}_\phi | \lambda_\phi \rangle = A \sqrt{\frac{3}{4\pi}} D_{\lambda_\phi 0}^1(\Omega_{K\bar{K}}) \quad (\text{B12})$$

and

$$\int d\Omega_{K\bar{K}} |\langle \Omega_{K\bar{K}} | \hat{T}_\phi | \lambda_\phi \rangle|^2 = |A|^2. \quad (\text{B13})$$

We can factor out $\int d\Omega_{K\bar{K}} |\langle \Omega_{K\bar{K}} | \hat{T}_\phi | \lambda_\phi \rangle|^2$ because it is independent of the value of λ_ϕ and obtain

$$N = \frac{1}{3} \sum_{\lambda'_\phi} \int d\Omega_{K\bar{K}} |\langle \Omega_{K\bar{K}} | \hat{T}_\phi | \lambda'_\phi \rangle|^2 \left[\frac{1}{2} \int du_\phi d\Omega_{pn} \frac{P_{pn}}{M_{pn}} |c|^2 \sum_{\lambda_\phi \lambda_p \lambda_n \lambda_\gamma \lambda_d} |\langle \lambda_\phi \lambda_p \lambda_n | \hat{T}_{\gamma d} | \lambda_\gamma \lambda_d \rangle|^2 \right], \quad (\text{B14})$$

where the summation over ϕ -meson helicity states λ'_ϕ and a factor of 1/3 are needed for comparison with Eq. (B8).

We can compare Eqs. (B10) and (B14) to Eqs. (B7) and (B8) to obtain

$$\rho_{\lambda_\phi \lambda'_\phi}(\phi) \equiv \frac{1}{N_{\gamma d}} \sum_{\lambda_p \lambda_n \lambda_d} \sum_{\lambda_\gamma \lambda'_\gamma} \int du_\phi d\Omega_{pn} \frac{P_{pn}}{M_{pn}} \langle \lambda_\phi \lambda_p \lambda_n | \hat{T}_{\gamma d} | \lambda_\gamma \lambda_d \rangle \rho_{\lambda_\gamma \lambda'_\gamma}(\gamma) \langle \lambda'_\gamma \lambda_d | \hat{T}_{\gamma d}^\dagger | \lambda'_\phi \lambda_p \lambda_n \rangle, \quad (\text{B15})$$

with

$$N_{\gamma d} \equiv \frac{1}{2} \int du_\phi d\Omega_{pn} \frac{P_{pn}}{M_{pn}} \times \sum_{\lambda_\phi \lambda_p \lambda_n \lambda_\gamma \lambda_d} |\langle \lambda_\phi \lambda_p \lambda_n | \hat{T}_{\gamma d} | \lambda_\gamma \lambda_d \rangle|^2. \quad (\text{B16})$$

APPENDIX C: RELATION BETWEEN SINGLE-SCATTERING DCSs AND THE DCSs WITH ON-SHELL pn FSI

Let us begin from the operator of the $\gamma d \rightarrow \phi pn$ reaction,

$$\hat{T} = \hat{T}_S + \hat{T}_{\text{FSI}}, \quad (\text{C1})$$

where the operator \hat{T}_S contains only single-scattering interactions, as represented in Fig. 2(a), and

$$-i\hat{T}_{\text{FSI}} = (-i\hat{T}_{pn}) \frac{i}{E - \hat{H} + i\epsilon} (-i\hat{T}_S), \quad (\text{C2})$$

in which the operator \hat{T}_{FSI} contains pn FSI only, as represented in Fig. 2(b). Here the total energy E of the final ϕ , p , and n is $E = E_{pn} + E_\phi$, where the energy of the proton and neutron in the final state $E_{pn} = E_p + E_n$. The free Hamiltonian of the particles in the intermediate state where proton, neutron, and

ϕ meson are not interacting is

$$\hat{H} = \hat{H}_{pn} + \hat{H}_\phi, \quad (\text{C3})$$

where \hat{H}_{pn} is just the free Hamiltonian of the pn system and $\hat{H}_\phi \rightarrow E_\phi$ as the ϕ meson is already in free space. Now, because

$$\frac{1}{E_{pn} - \hat{H}_{pn} + i\epsilon} = \mathcal{P} \frac{1}{E_{pn} - \hat{H}_{pn}} - i\pi \delta(\Delta E_{pn}), \quad (\text{C4})$$

Eq. (C2) can be rewritten as

$$\hat{T}_{\text{FSI}} = \hat{T}_{\text{FSI, off}} + \hat{T}_{\text{FSI, on}}. \quad (\text{C5})$$

However, let us focus on the amplitude calculated within the on-shell approximation, or

$$\hat{T}_{\text{on}} = \hat{T}_S + \hat{T}_{\text{FSI, on}}, \quad (\text{C6})$$

where again the subscript on the full operator \hat{T}_{on} is to denote that the on-energy-shell approximation has been taken, and in which

$$\hat{T}_{\text{FSI, on}} \equiv \hat{T}_{pn} [-i\pi \delta(\Delta E_{pn})] \hat{T}_S. \quad (\text{C7})$$

where the operator \hat{T}_{pn} is defined for elastic pn scattering in which the initial and final states are both on energy shell and ΔE_{pn} is the difference of the on-shell energies between the two states.

Here we need to have some basic relations between the amplitudes involved in pn scattering. The scattering operator

$$\hat{S}_{pn} = \hat{1} + 2\pi\delta(\Delta E_{pn})(-i\hat{T}_{pn}) \quad (\text{C8})$$

obeys the unitarity relation

$$\hat{S}_{pn}\hat{S}_{pn}^\dagger = \hat{S}_{pn}^\dagger\hat{S}_{pn} = \hat{1}, \quad (\text{C9})$$

which also implies that

$$\hat{T}_{pn}\hat{T}_{pn}^\dagger = \hat{T}_{pn}^\dagger\hat{T}_{pn}. \quad (\text{C10})$$

Having all these relations, we can continue to calculate the operator \hat{T}_{on} ,

$$\hat{T}_{\text{on}} = \hat{T}_S + \hat{T}_{pn}[-i\pi\delta(\Delta E_{pn})]\hat{T}_S = \frac{1}{2}(\hat{1} + \hat{S}_{pn})\hat{T}_S. \quad (\text{C11})$$

Now we are ready to calculate $\hat{T}_{\text{on}}^\dagger\hat{T}_{\text{on}}$,

$$\begin{aligned} \hat{T}_{\text{on}}^\dagger\hat{T}_{\text{on}} &= \frac{1}{4}\hat{T}_S^\dagger(\hat{1} + \hat{S}_{pn}^\dagger)(\hat{1} + \hat{S}_{pn})\hat{T}_S \\ &= \frac{1}{4}\hat{T}_S^\dagger[4\hat{1} - 2i\pi\delta(\Delta E_{pn})\hat{T}_{pn} + 2i\pi\delta(\Delta E_{pn})\hat{T}_{pn}^\dagger]\hat{T}_S, \end{aligned} \quad (\text{C12})$$

where the last line is reached by using Eqs. (C8) and (C9). We can continue

$$\begin{aligned} \hat{T}_{\text{on}}^\dagger\hat{T}_{\text{on}} &= \hat{T}_S^\dagger[\hat{1} - \frac{1}{2}i\pi\delta(\Delta E_{pn})\hat{T}_{pn} + \frac{1}{2}i\pi\delta(\Delta E_{pn})\hat{T}_{pn}^\dagger]\hat{T}_S \\ &= \hat{T}_S^\dagger\hat{T}_S + \frac{1}{2}\hat{T}_S^\dagger\hat{T}_{pn}[-i\pi\delta(\Delta E_{pn})]\hat{T}_S \\ &\quad + \frac{1}{2}\hat{T}_S^\dagger[i\pi\delta(\Delta E_{pn})]\hat{T}_{pn}^\dagger\hat{T}_S \\ &= \hat{T}_S^\dagger\hat{T}_S + \frac{1}{2}(\hat{T}_S^\dagger\hat{T}_{\text{FSI, on}} + \hat{T}_{\text{FSI, on}}^\dagger\hat{T}_S). \end{aligned} \quad (\text{C13})$$

Finally, by using

$$\begin{aligned} \hat{T}_{\text{on}}^\dagger\hat{T}_{\text{on}} &= (\hat{T}_S^\dagger + \hat{T}_{\text{FSI, on}}^\dagger)(\hat{T}_S + \hat{T}_{\text{FSI, on}}) \\ &= \hat{T}_S^\dagger\hat{T}_S + \hat{T}_{\text{FSI, on}}^\dagger\hat{T}_{\text{FSI, on}} + \hat{T}_S^\dagger\hat{T}_{\text{FSI, on}} + \hat{T}_{\text{FSI, on}}^\dagger\hat{T}_S \end{aligned} \quad (\text{C14})$$

to substitute the second term in the round brackets of the last line of Eq. (C13), we have, from Eq. (C13),

$$\hat{T}_{\text{on}}^\dagger\hat{T}_{\text{on}} = \hat{T}_S^\dagger\hat{T}_S - \hat{T}_{\text{FSI, on}}^\dagger\hat{T}_{\text{FSI, on}}. \quad (\text{C15})$$

Now we must be very careful in interpreting this apparently simple formula. It has to be understood that this equation consists of operators and can be related to amplitudes only after we apply a suitable set of states onto them. This procedure also includes an application of a completeness relation between the operators. The completeness relation in this case must be constructed from the states present in the S matrix \hat{S}_{pn} , which when applied to the operators provides a summation over the spins and an integration over the solid angles of the proton and neutron. The resulting quantities will be proportional to the DCSs of incoherent ϕ -meson photoproduction in which the momenta and spins of the outgoing proton and neutron are not observed,

$$\frac{d\sigma_{\text{total, on}}}{dt} = \frac{d\sigma_S}{dt} - \frac{d\sigma_{\text{FSI, on}}}{dt}, \quad (\text{C16})$$

which proves the statement stated before. Notice that unitarity relation for the pn system in the final state given in Eq. (C9) actually plays an important role in the derivation.

-
- [1] T. H. Bauer, R. D. Spital, D. R. Yennie, and F. M. Pipkin, *Rev. Mod. Phys.* **50**, 261 (1978).
- [2] A. Donnachie and P. V. Landshoff, *Phys. Lett. B* **185**, 403 (1987); *Nucl. Phys. B* **244**, 322 (1984); **267**, 690 (1986); **311**, 509 (1989).
- [3] R. A. Williams, *Phys. Rev. C* **57**, 223 (1998).
- [4] Y. S. Oh and H. C. Bhang, *Phys. Rev. C* **64**, 055207 (2001).
- [5] Q. Zhao, J.-P. Didelez, M. Guidal, and B. Saghai, *Nucl. Phys. A* **660**, 323 (1999); Q. Zhao, B. Saghai, and J. S. Al-Khalili, *Phys. Lett. B* **509**, 231 (2001).
- [6] A. I. Titov and T.-S. H. Lee, *Phys. Rev. C* **67**, 065205 (2003).
- [7] A. I. Titov, T.-S. H. Lee, H. Toki, and O. Streltsova, *Phys. Rev. C* **60**, 035205 (1999).
- [8] A. I. Titov, Y. S. Oh, and S. N. Yang, *Phys. Rev. Lett.* **79**, 1634 (1997); A. I. Titov, Y. S. Oh, S. N. Yang, and T. Morii, *Phys. Rev. C* **58**, 2429 (1998); *Nucl. Phys. A* **684**, 354 (2001).
- [9] A. I. Titov, S. N. Yang, and Y. S. Oh, *Nucl. Phys. A* **618**, 259 (1997); Y. S. Oh, A. I. Titov, S. N. Yang, and T. Morii, *Phys. Lett. B* **462**, 23 (1999).
- [10] T. Mibe *et al.* (LEPS Collaboration), *Phys. Rev. Lett.* **95**, 182001 (2005), and references therein.
- [11] B. Dey *et al.* (CLAS Collaboration), *Phys. Rev. C* **89**, 055208 (2014).
- [12] H. Seraydaryan *et al.* (CLAS Collaboration), *Phys. Rev. C* **89**, 055206 (2014).
- [13] A. Kiswandhi, J. J. Xie, and S. N. Yang, *Phys. Lett. B* **691**, 214 (2010).
- [14] A. Kiswandhi and S. N. Yang, *Phys. Rev. C* **86**, 015203 (2012).
- [15] W. C. Chang *et al.* (LEPS Collaboration), *Phys. Rev. C* **82**, 015205 (2010).
- [16] W. C. Chang *et al.* (LEPS Collaboration), *Phys. Lett. B* **684**, 6 (2010).
- [17] X. Qian *et al.* (CLAS Collaboration), *Phys. Lett. B* **696**, 338 (2011).
- [18] T. Sekihara, A. M. Torres, D. Jido, and E. Oset, *Eur. Phys. J. A* **48**, 10 (2012).
- [19] J. J. de Swart, R. A. M. M. Klomp, M. C. M. Rentmeester, and Th. A. Rijken, *Few-Body Syst. Suppl.* **8**, 438 (1995).
- [20] Calculations of the observables using the Nijmegen potential were done using the NNOnline website and is the work of the Theoretical High Energy Physics Group of the Radboud University Nijmegen, the Netherlands, on the website (<http://nn-online.org/NN/>).
- [21] S. Capstick, *Phys. Rev. D* **46**, 2864 (1992).
- [22] A. Kiswandhi, Y. B. Dong, and S. N. Yang, *EPJ Web Conf.* **73**, 04008 (2014).
- [23] R. Machleidt, *Phys. Rev. C* **63**, 024001 (2001).
- [24] A. Sibirtsev, H.-W. Hammer, U.-G. Meissner, and A. W. Thomas, *Eur. Phys. J. A* **29**, 209 (2006).
- [25] J. J. Xie, B. S. Zou, and H. C. Chiang, *Phys. Rev. C* **77**, 015206 (2008).
- [26] W. C. Chang (private communication).
- [27] D. E. Groom *et al.* (Particle Data Group), *Eur. Phys. J. C* **15**, 1 (2000).

- [28] A. I. Titov, T. Nakano, S. Date, and Y. Ohashi, *Phys. Rev. C* **76**, 048202 (2007).
- [29] A. I. Titov and B. Kämpfer, *Phys. Rev. C* **76**, 035202 (2007).
- [30] W.-T. Chiang, S. N. Yang, M. Vanderhaeghen, and D. Drechsel, *Nucl. Phys. A* **723**, 205 (2003).
- [31] T. Feuster and U. Mosel, *Nucl. Phys. A* **612**, 375 (1997).
- [32] V. Pascalutsa, M. Vanderhaeghen, and S. N. Yang, *Phys. Rep.* **437**, 125 (2007).
- [33] C.-T. Hung, S. N. Yang, and T.-S. H. Lee, *Phys. Rev. C* **64**, 034309 (2001).
- [34] K. Schilling, K. Seyboth, and G. Wolf, *Nucl. Phys. B* **15**, 397 (1970).